Downloaded from gsabulletin.gsapubs.org on November 12, 2010

ENTERED

Geological Society of America Bulletin

# Orthogonal jointing during coeval igneous degassing and normal faulting, Yucca Mountain, Nevada

William M. Dunne, David A. Ferrill, Juliet G. Crider, Brittain E. Hill, Deborah J. Waiting, Peter C. La Femina, Alan P. Morris and Randall W. Fedors

*Geological Society of America Bulletin* [redacted] 115;1492-1509
doi: 10.1130/B25231.1

**Email alerting services** click www.gsapubs.org/cgi/alerts to receive free e-mail alerts when new articles cite this article

**Subscribe** click www.gsapubs.org/subscriptions/ to subscribe to Geological Society of America Bulletin

**Permission request** click http://www.geosociety.org/pubs/copyrt.htm#gsa to contact GSA

Copyright not claimed on content prepared wholly by U.S. government employees within scope of their employment. Individual scientists are hereby granted permission, without fees or further requests to GSA, to use a single figure, a single table, and/or a brief paragraph of text in subsequent works and to make unlimited copies of items in GSA's journals for noncommercial use in classrooms to further education and science. This file may not be posted to any Web site, but authors may post the abstracts only of their articles on their own or their organization's Web site providing the posting includes a reference to the article's full citation. GSA provides this and other forums for the presentation of diverse opinions and positions by scientists worldwide, regardless of their race, citizenship, gender, religion, or political viewpoint. Opinions presented in this publication do not reflect official positions of the Society.

**Notes**

Geological Society of America

THE GEOLOGICAL SOCIETY OF AMERICA

34102

Downloaded from gsabulletin.gsapubs.org on November 12, 2010

# Orthogonal jointing during coeval igneous degassing and normal faulting, Yucca Mountain, Nevada

**William M. Dunne**†
*Department of Geological Sciences, University of Tennessee, Knoxville, Tennessee 37996, USA*

**David A. Ferrill**
*Center for Nuclear Waste Regulatory Analyses, Southwest Research Institute, San Antonio, Texas 78238, USA*

**Juliet G. Crider**
*Department of Geology, Western Washington University, Bellingham, Washington 98225, USA*

**Brittain E. Hill**
**Deborah J. Waiting**
**Peter C. La Femina**
*Center for Nuclear Waste Regulatory Analyses, Southwest Research Institute, San Antonio, Texas 78238, USA*

**Alan P. Morris**
*Department of Earth and Environmental Sciences, University of Texas, San Antonio, Texas 78249, USA*

**Randall W. Fedors**
*Center for Nuclear Waste Regulatory Analyses, Southwest Research Institute, San Antonio, Texas 78238, USA*

## ABSTRACT

**An orthogonal system of tube-bearing joints constitutes the oldest fractures in the Tiva Canyon Tuff at Yucca Mountain, Nevada. The joints formed within a month of ignimbrite deposition, prior to major degassing. The system consists of (1) narrow, persistent, northeast-striking joint swarms with trace lengths typically greater than 5 m and between-joint spacings of less than 20 cm and (2) northwest-striking swarms that have a more en echelon geometry and greater between-joint spacings compared to the northeast-striking swarms. Between-swarm spacing for both trends is ~50 m. Questions concerning the joints include the following: (1) What was the origin of driving stress(es) for formation of the joints, particularly as their orientations were not consistent with the regional stress geometry at the time of their formation? (2) What mechanism caused the horizontal principal stresses to be reoriented so as to yield an orthogonal geometry? (3) What insights can be developed for predicting joint geometry in unexposed rock volumes by understanding joint origin? These questions are important because the joints and other fractures may affect the performance of a proposed high-level nuclear waste repository within Yucca Mountain.**

**To address these questions, we use new and existing field data about joint geometry and the relationships of joints to degassing structures, numerical modeling of fault behavior, and work by previous authors. Our interpretation begins with the initial ignimbrite eruption and deposition during caldera collapse. The ignimbrites were deposited over a preexisting topography that possibly included a shallow northwest-trending basin in the Yucca Mountain area. During initial ignimbrite cooling, joint swarms formed as elements of orthogonal fumarolic ridge systems where degassing was associated with vertical dilation. Both joint sets have unusual tubes that are interpreted to have formed during dilation and segmentation of joint faces resulting from lithophysae inflation in the cooling ignimbrite deposit. Modeling supports the interpretation that a combination of regional stresses and stress related to slip on local normal faults controlled the orientation of the joint swarms and favored the formation of the northeast-striking joints first. The faults might have moved in a stress field already perturbed by caldera collapse. Formation of the northwest-striking joints occurred after a local 90° switch of horizontal principal stress directions due to the presence of the northeast-striking swarms, possibly aided by differential compaction across the northwest-trending basin. Tube-bearing joints occur in all lithophysae-bearing lithostratigraphic units of the Topopah Spring Tuff, which is the stratigraphic interval for the proposed nuclear waste repository within Yucca Mountain. We conclude that the tube-bearing joints formed in the same manner and share similar geometric characteristics, adding a persistent joint population to the overall fracture system that influences hydrological and mechanical properties.**

**Keywords: orthogonal joints, welded tuffs, cooling joints, degassing tubes, perturbed stress fields, normal faults.**

## INTRODUCTION

We consider the origin of tube-bearing joints in the Miocene Tiva Canyon Tuff (12.7 Ma) and extrapolate the study to other tube-bearing joints at Yucca Mountain, Nevada.

†E-mail: wdunne@utk.edu.

*GSA Bulletin*; December 2003; v. 115; no. 12; p. 1492–1509; 9 figures; 1 table; Data Repository item 2003168.



For permission to copy, contact editing@geosociety.org
© 2003 Geological Society of America

Downloaded from gsabulletin.gsapubs.org on November 12, 2010


The faces of tube-bearing joints are distinctively ornamented by a network of linear depressions with curved bottoms (Figs. 1A, 1B) that are symmetrical across the two faces of a joint. The tube-bearing joint system is intriguing because (1) two nearly orthogonal joint sets define the system, (2) both joint sets are clearly associated with ignimbrite degassing, and (3) neither joint set is perpendicular to the approximately east-west direction of regional extension at the time of both sets' formation (Zoback et al., 1981; Morris et al., 1996). Thus, the joints formed during ignimbrite cooling in response to additional stress components that do not reflect the regional stress field. These stress components also triggered a 90° switch of horizontal stress directions that produced both sets of the near-orthogonal system.

The joint system is also of interest because it is located above the proposed site for the United States of America's first high-level radioactive-waste repository in Yucca Mountain, Nevada. The joint system is a prominent component of the pathways for shallow groundwater infiltration through the capping, moderately to densely welded tuff into the repository (Winograd, 1971; Flint and Flint, 1995; Buesch et al., 1996; Flint et al., 1996). Joints with morphologies similar to those exposed at the surface of Yucca Mountain are also found in subsurface exposures in the Exploratory Studies Facility (ESF) and Enhanced Characterization of the Repository Block (ECRB) tunnels (Mongano et al., 1999; CRWMS M and O [Civilian Radioactive Waste Management System Management and Operating Contractor], 2000). Joints that we interpret to have formed early in the welded ignimbrites tend to be relatively large and represent potential weaknesses that could influence the stability of proposed excavations such as underground waste-emplacement drifts. A better understanding of the geometry and origin of these joints provides a basis for better estimating their importance to the design of underground openings.

In this paper, we (1) provide a summary of the joint formation history based on new analyses and published information for the degassing-related joints in a part of the Tiva Canyon Tuff; (2) identify the sources of the driving stresses that may have perturbed the regional stress field to form this orthogonal joint system; and (3) consider causes for the 90° switch of horizontal stress directions that caused the orthogonal geometry. Although the analysis is conducted in volcanic rocks, the results are applicable to faulted sedimentary rocks with elevated fluid pressures. To analyze the origin of this joint system, we have used existing field data (e.g., Morgan, 1984; Barton et al., 1984, 1993; Barton and Larsen, 1985; Sweetkind et al., 1995a, 1995b; Throckmorton and Verbeek, 1995), newly gathered field-based fracture data employing a differential Global Positioning System (GPS) and geographic information system (GIS) approach, new observations of field relationships between joints and volcanogenic features, and numerical modeling of stress-field perturbation during active faulting.

## DEVELOPING ORTHOGONAL JOINT SYSTEMS

Orthogonal systems of two vertical joint sets are common (Ver Steeg, 1942; Eyal and Reches, 1983; Hancock, 1985; Stauffer and Gendzwill, 1987; Dunne and North, 1990; Rawnsley et al., 1992; Martel, 1994; Caputo, 1995; Olson, 1996; Fabbri et al., 2001). Nevertheless, our understanding of their origin is problematic because the orthogonal geometry of the two sets requires at least one 90° change in local principal stress directions during joint system formation, so that each set forms normal to the minimum principal compressive stress. Specifically, the minimum horizontal stress direction ($S_h$) must change by 90° or switch with the direction of maximum horizontal stress ($S_H$). Three groups of mechanisms have been proposed (Lachenbruch, 1962; Stauffer and Gendzwill, 1987; Dunne and North, 1990; Caputo, 1995; Olson, 1996): (1) reorienting due to small stress fluctuations between two near-equal horizontal principal stresses ($S_h \approx S_H$), (2) local stress switching at the scale of individual joints, and (3) regional stress switching by 90°. Switching two nearly equal horizontal principal stresses is an intuitively simple scenario because little change is required in the stress conditions to generate the new stress geometry. Yet, when these two stresses are nearly equal, joints may form in more than one orientation because horizontal stress conditions are essentially isotropic, which leads to the formation of random or columnar cooling joints (Lachenbruch, 1962; Pollard and Aydin, 1988) rather than orthogonal joints. Thus, this stress state is unlikely to yield the orthogonal geometry. Recent numerical modeling has shown that local stress switching is plausible and could occur as a consequence of close spacing in layer-bounded joints (Bai et al., 2002), although initial analysis by Martel (1994) indicated only limited potential. Regional switching may occur as a result of regional tectonic changes in stress state over time or relaxation of stresses as a result of uplift and erosion (Engelder, 1985; Hancock, 1985; Stauffer and Gendzwill, 1987; Dunne and North, 1990; Rives et al., 1994; Caputo, 1995). These switches do not have to occur in a short timeframe, which means that two joint sets with an orthogonal geometry may each form at different times in response to unrelated stress regimes (Gross, 1993; Rawnsley et al., 1998). Thus, both local-scale and regional switching mechanisms may each account for the formation of some orthogonal joint systems.

At Yucca Mountain, identification of the most likely mechanism and scale for triggering changes in stress orientation that formed the orthogonal joint network is needed. A variety of volcanic and tectonic driving stresses is feasible: (1) the region was actively extending; (2) a large-scale caldera eruption had just occurred; (3) the ignimbrite containing the joints was still cooling, probably with different temperature gradients through the deposit; (4) the ignimbrite may have compacted differentially during joint formation; and (5) normal faults near Yucca Mountain could have moved seismically at that time. Considering the relative roles of these factors during joint formation is necessary to understanding the mechanisms affecting stress orientations.

## REGIONAL GEOLOGY

### Tectonic Setting

The orthogonal joint system of interest is in the welded ignimbrites of the Miocene Tiva Canyon Tuff, which was emplaced across the location of the present Yucca Mountain in southwestern Nevada at 12.7 Ma (Fig. 2A). Yucca Mountain consists of a thick accumulation of gently east-dipping Miocene tuff deposits cut by an array of major north-striking, west-dipping normal faults, such as the Solitario Canyon, Bow Ridge, and Paintbrush Canyon faults, and northwest-striking dextral strike-slip faults (Scott and Bonk, 1984; Day et al., 1998a, 1998b; Ferrill et al., 1996a, 1999a; Ferrill and Morris, 2001). These faults accommodated active crustal extension within the Basin and Range province through the Cenozoic to the present day (Scott, 1990; Wernicke, 1992; Axen et al., 1993; Morris et al., 1996; Day et al., 1998a).

Although this period of tectonic activity includes the time of Tiva Canyon Tuff volcanism, data supporting fault displacements coeval with volcanism and cooling are limited. The Solitario Canyon fault has several splay faults that exhibit displacement that decreases upward to fault tips in the Tiva Canyon Tuff (Day et al., 1998a), which are interpreted to result from normal faulting after or during deposition of the Tiva Canyon Tuff (Day et al.,

Downloaded from gsabulletin.gsapubs.org on November 12, 2010


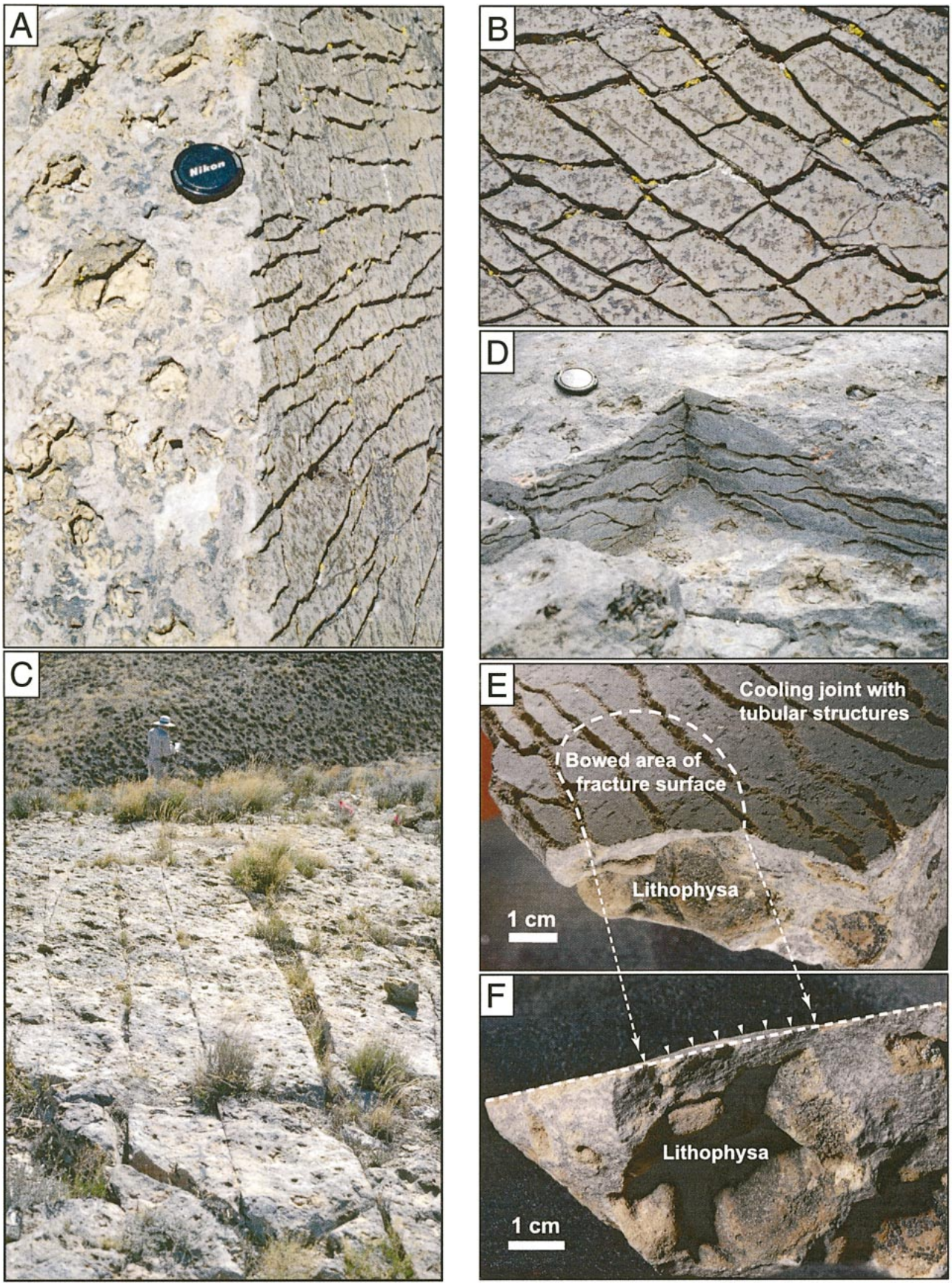

Downloaded from gsabulletin.gsapubs.org on November 12, 2010


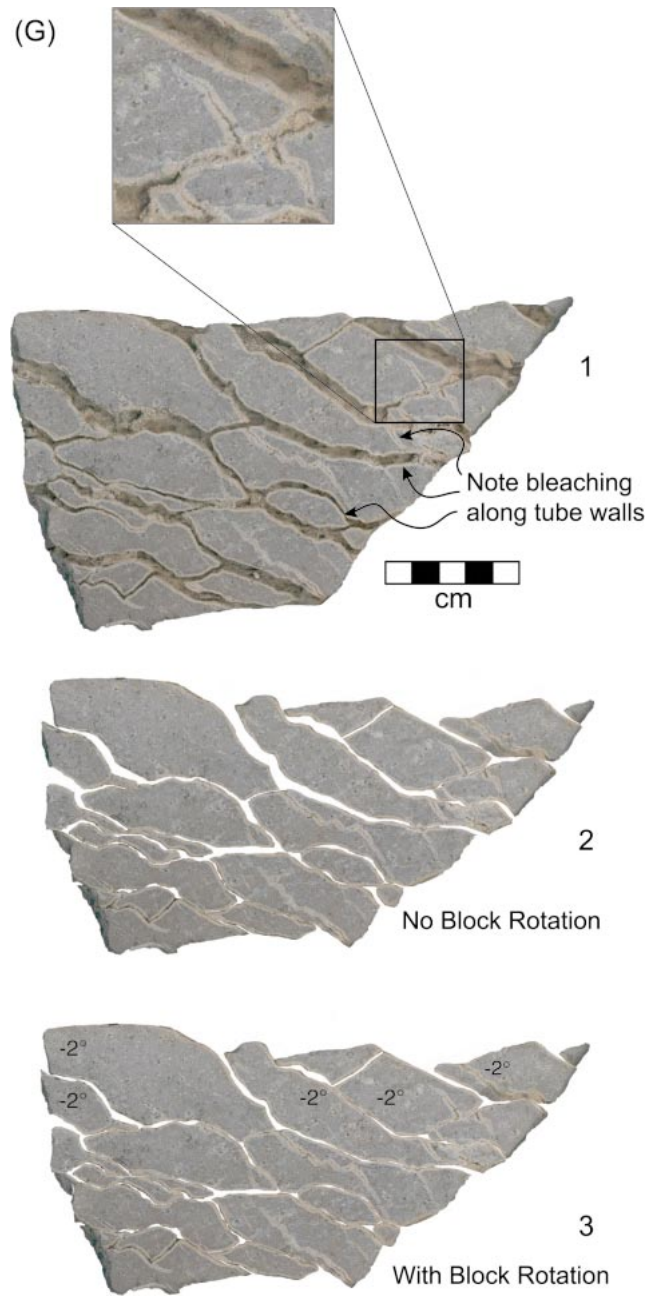


**Figure 1. (*Continued.*)**

**Figure 1. Photographs of joints in the upper lithophysae-bearing unit of the Tiva Canyon Tuff. (A) Smooth cooling joint with tubular structures defines one face of loose block (right side of photo), and later joint (at ~90°) with rougher surface morphology cuts lithophysae (left side of photo). (B) Tubular structures on cooling joint surface shown in A. (C) Cooling joint swarm on pavement P100 (view toward the southwest). (D) Intersection of two cooling joints on pavement P100. (E) Oblique view of hand sample showing smooth cooling joint with tubular structures that are bowed adjacent to ~5-cm-diameter lithophysa. (F) View parallel to main cooling joint surface in E shows deflection or bowing (arrows) of joint surface from overall planar geometry (dashed line). Total deflection is ~2 mm. Note in E and F that deflection of the cooling joint surface locally occurs as discrete steps across tubular structures. (G1) Detail of smooth cooling joint with tubular structures. Inset shows small-aperture fractures and large-aperture tubes cutting one face of a cooling joint. Tubes and fracture tips have bleached walls. The expanded image shows fractures with apertures ranging from <1 mm at fracture tips to nearly 1 cm along major tubes. Regardless of aperture, fracture walls show bleaching indicative of vapor-phase mineralization and alteration of adjacent rock. Unbleached areas away from tube-bearing joints are part of the vertical joint surface that would have been forced tightly closed by lateral stress caused by gas expansion and formation of lithophysae. (G2) Restoration of tubes shown in G1 by matching sides to show volume increase using block translation without rotation. (G3) Restoration of tubes shown in G1 by matching sides to show volume increase using block translation with minor rotation (counterclockwise indicated by −2°) of some blocks.**

1998a). From unpublished subsurface thickness data, Fridrich (1999) stated that some of the major north-striking faults in the Yucca Mountain region were active between 13.1 and 12.7 Ma, including the time of eruption for the Tiva Canyon Tuff. Finally, significant normal-fault displacements occurred during the million years after deposition of the Tiva Canyon Tuff, on the basis of abrupt changes in thickness of the overlying 11.6 Ma Rainier Mesa Tuff where it crosses faults (e.g., Christiansen et al., 1977; Sawyer et al., 1994; Monsen et al., 1992; Day et al., 1998a; Fridrich, 1999).

## Volcanic Setting

The Tiva Canyon Tuff of the Paintbrush Group is a sequence of pyroclastic flow and minor tephra-fall deposits that most likely erupted from the Claim Canyon caldera, which is partly preserved on the southern edge of the younger Timber Mountain caldera complex (Fig. 2B, Table 1) (Byers et al., 1976; Buesch et al., 1996; Potter et al., 2002). The Tiva Canyon Tuff consists mostly of moderately to densely welded ignimbrites with devitrification, welding, and vapor-phase alteration features that resulted from the eruption of at least 1000 km$^3$ of compositionally zoned rhyolitic magma at 12.7 ± 0.03 Ma (Byers et al., 1976; Sawyer et al., 1994). The ~100-m-thick Tiva Canyon Tuff has two lithostratigraphic members: a thin, crystal-rich upper member and a thick, crystal-poor lower member (Buesch et al., 1996). These members form a single cooling unit (Rosenbaum, 1986). Our study was conducted within the

Downloaded from gsabulletin.gsapubs.org on November 12, 2010


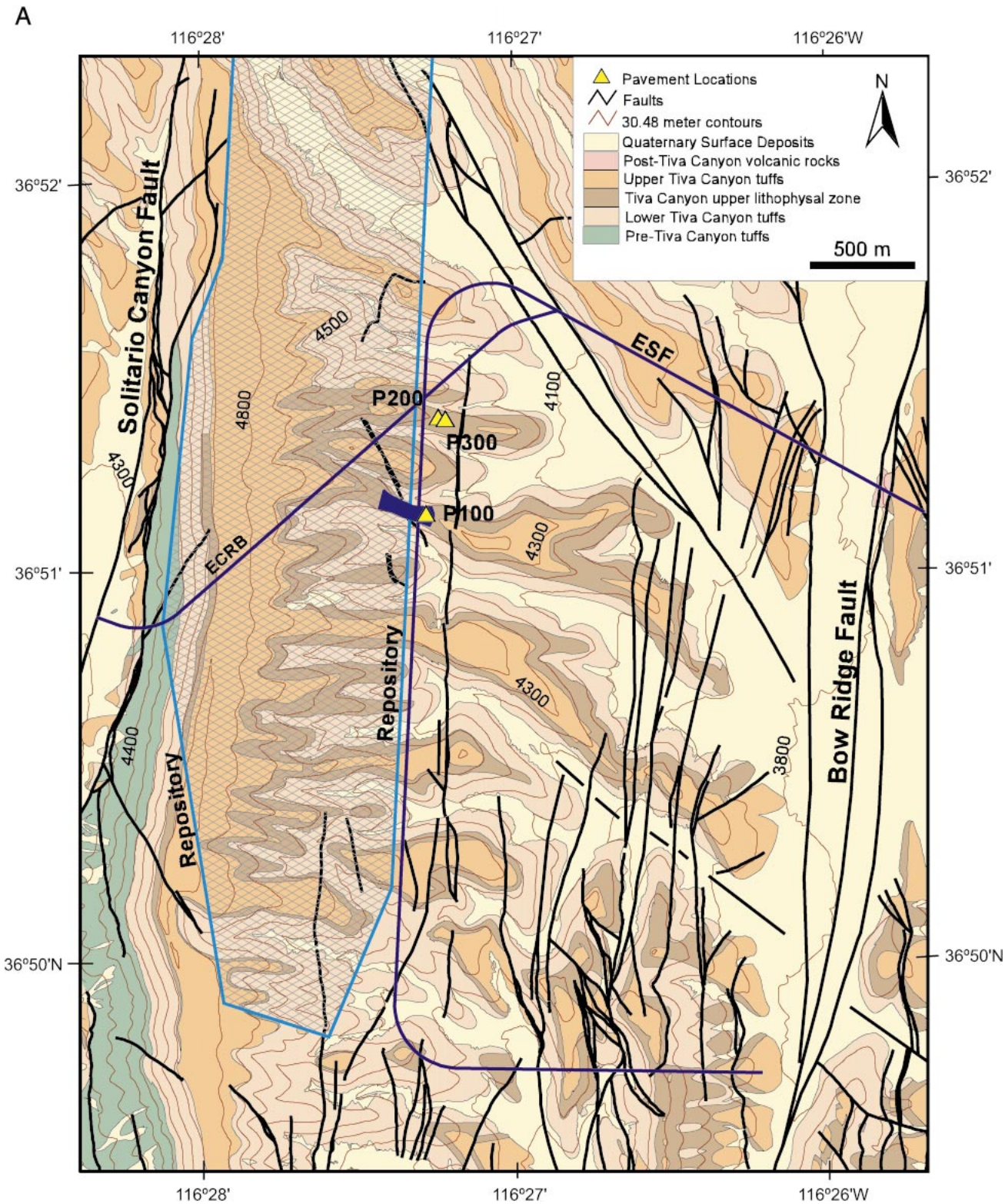


**Figure 2. (A) Geologic map of Yucca Mountain, Nevada. Map is based on geologic mapping of Day et al. (1998b) and shows proposed repository outline (bright blue), topographic contours, distribution of Tiva Canyon Tuff, Exploratory Studies Facility (ESF) tunnel (projected surface trace shown by dark blue line), Enhanced Characterization of the Repository Block tunnel (ECRB) (projected surface trace shown by dark blue line); locations of pavements P100, P200, and P300; and the joint study area (dark blue rectangle) on Live Yucca Ridge. Repository area shown by cross-hatching. (B) Regional map showing location of Yucca Mountain with respect to Fran Ridge and the caldera complexes to the north. Base image is Landsat 5–Thematic Mapper acquired from the U.S. Geological Survey. Caldera coverage from Frizzell and Shulters (1990). Maps in both A and B are in Universal Transverse Mercator (UTM), Zone 11, North American Datum 1927 (NAD27).**

Downloaded from gsabulletin.gsapubs.org on November 12, 2010


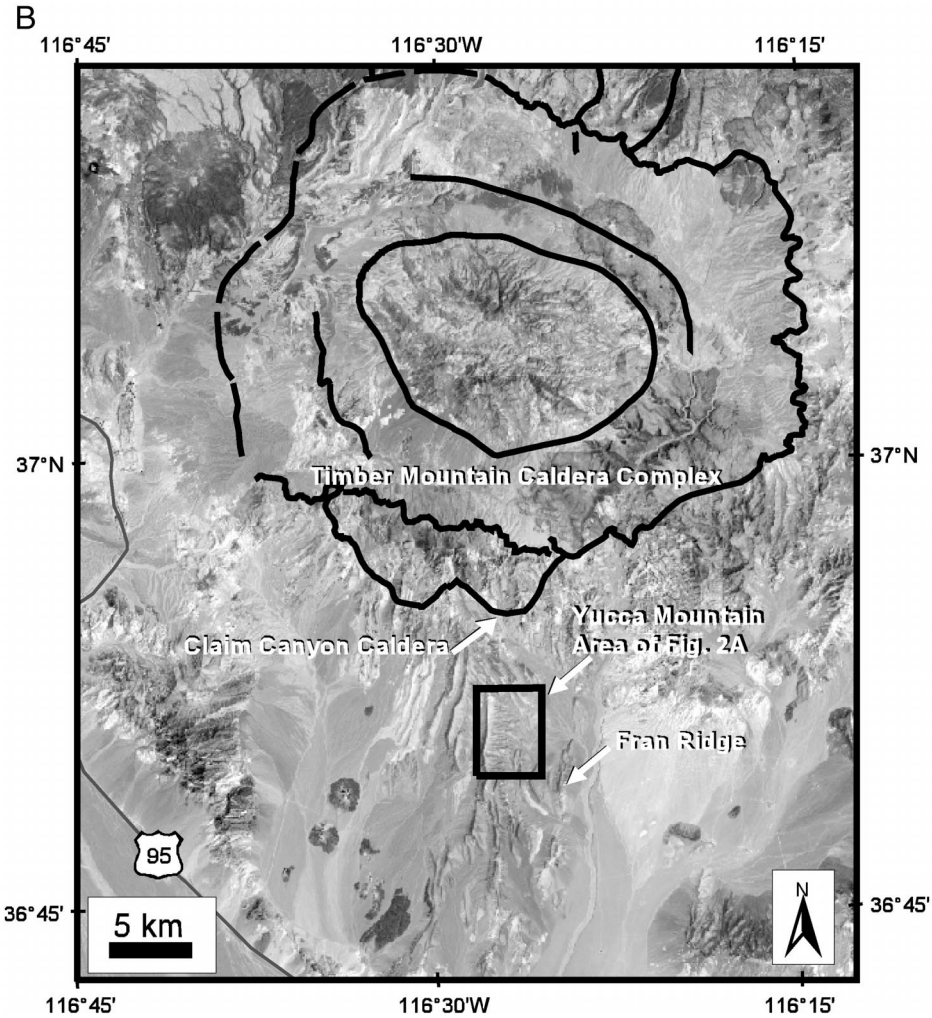


**Figure 2. (*Continued.*)**

TABLE 1. STRATIGRAPHIC COLUMN FOR YUCCA MOUNTAIN

| Formation | Age (Ma) |
|---|---|
| Timber Mountain Group | |
| Rainier Mesa Tuff | 11.6 |
| Paintbrush Canyon Group | |
| Bedded Tuff | |
| Tiva Canyon Tuff | 12.7 |
| Yucca Mountain Tuff | |
| Pah Canyon Tuff | |
| Topopah Spring Tuff | 12.8 |
| Calico Hills Formation | 12.9 |
| Crater Flat Group | |
| Prow Pass Tuff | |
| Bullfrog Tuff | 13.25 |
| Tram Tuff | >13.5 |

*Note*: After Sawyer et al. (1994).

20-m-thick upper lithophysae-bearing zone of the crystal-poor member (Buesch et al., 1996).

Variations in preemplacement topography and depositional thickness affect the cooling behavior of ignimbrites and potentially affect their fracture development. The base of the Tiva Canyon Tuff is poorly exposed, so preemplacement topography is difficult to identify. Also, the top of the Tiva Canyon Tuff is eroded, obscuring its thickness variations. Still, the spatial distribution of stratigraphic thicknesses for underlying tuffs from the Paintbrush Group may indicate the location of depocenters for the younger Tiva Canyon (Buesch and Spengler, 1998; Fridrich, 1999). If it is assumed that the ignimbrite tops were flat after deposition, a northwest-striking basin for the underlying Topopah Spring Tuff lies directly north of the study area where the unit thickens 50 m into the depocenter. The small-volume Yucca Mountain and Pah Canyon Tuffs, which are immediately underneath the Tiva Canyon Tuff, also show the effects of a northwest-trending paleobasin and depositional control from a gentle topographic high that limited ignimbrite deposition immediately to the south (e.g., Day et al., 1998b; Fridrich, 1999).

## Processes of Ignimbrite Cooling

Ignimbrite deposits analogous to the Tiva Canyon Tuff are commonly emplaced at temperatures within 100 °C of magmatic temperatures, because little cooling occurs during flow except near the basal and upper contacts of the unit (Banks and Hoblitt, 1981; Bursik and Woods, 1996). The Tiva Canyon Tuff likely had a preeruption temperature of ~700 °C (Lipman and Friedman, 1975). Uniform paleomagnetic directions in the Tiva Canyon Tuff indicate emplacement temperatures above a Curie temperature between 580 and 640 °C and that any potential rheomorphic deformation occurred above the Curie temperature (Rosenbaum, 1986, 1993).

Degassing occurs rapidly during and after ignimbrite emplacement at a rate largely controlled by variations in permeability (Miller, 1990; Riehle et al., 1995). Gas pressures initially exceed lithostatic in the upper third of a tuff (Riehle et al., 1995). Trapped gas can form lithophysal cavities through matrix expansion or form other gas-escape structures along pathways to the surface. Gas pressures within an ignimbrite deposit likely fall below lithostatic within one month after emplacement (Riehle et al., 1995). Gases continue to evolve from the devitrification of volcanic glass through crystallization of anhydrous minerals (e.g., Smith, 1960), triggering vapor-phase crystallization in ignimbrites with matrix porosities greater than ~20% (Sheridan, 1970; Ragan and Sheridan, 1972). Subsequent devitrification and vapor-phase alteration continue to temperatures as low as 240 °C. Cooling to this temperature in the upper third of the Tiva Canyon Tuff probably occurred several years after emplacement (i.e., Lofgren, 1971; Riehle et al., 1995).

The timing of joint development can be evaluated by using features related to postdepositional cooling of the ignimbrite. Earliest-formed joints would be associated with gas-escape structures such as fumaroles, which occur with noticeable alteration mineralization (e.g., Sheridan, 1970; Hildreth, 1983; Keith, 1991; Buesch et al., 1999). Inflationary structures such as lithophysae also form in the earliest stage of degassing. Joints that form before the lithophysae would seldom cut or terminate in lithophysae, may be bent by rheomorphic deformation during lithophysae formation, and would show the effects of vapor-phase mineralization on the joint faces. Compaction and welding in ignimbrites analogous to Tiva Canyon Tuff typically continue for periods on the order of 1 to 10 yr (Friedman et al., 1963; Riehle, 1973; Bierwirth, 1982, cited in Cas and Wright, 1987; Riehle

Downloaded from gsabulletin.gsapubs.org on November 12, 2010


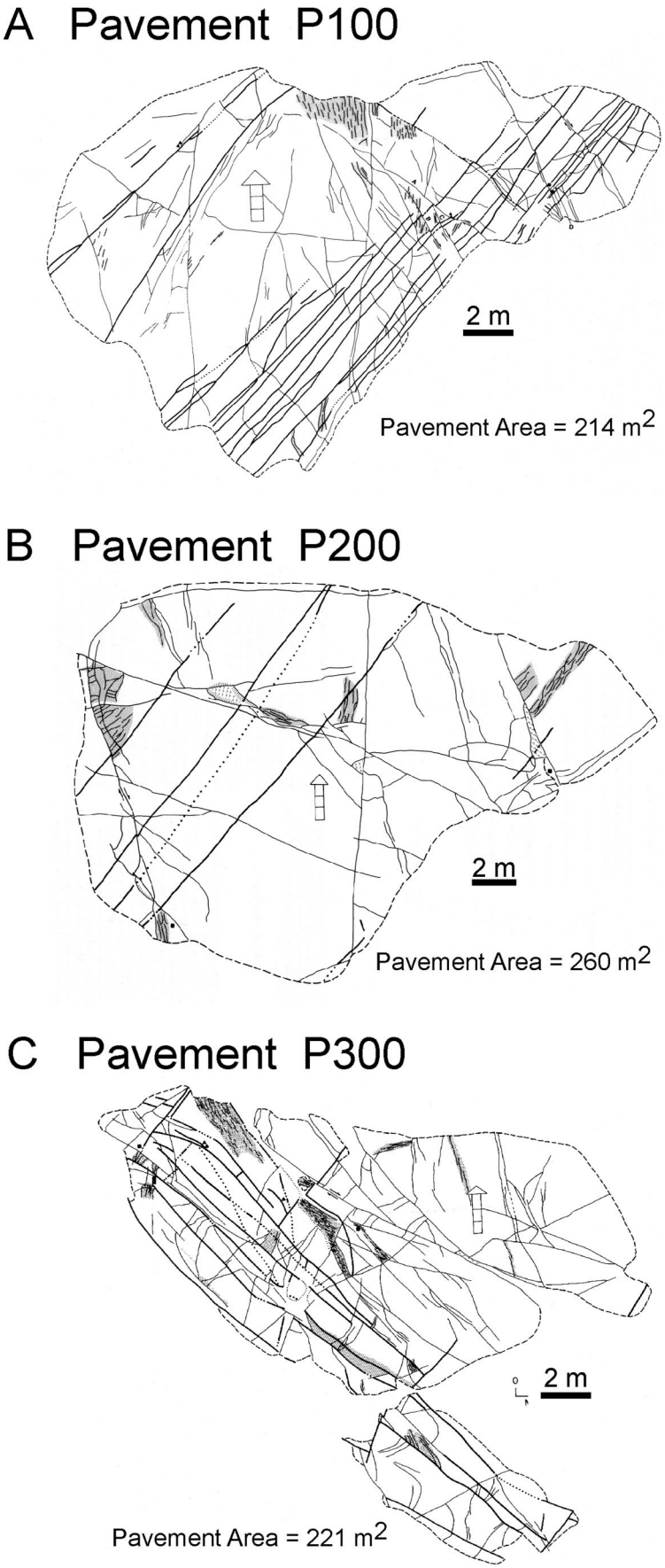


**Figure 3. Fracture and joint trace maps (modified from Barton et al., 1993) for cleared pavements in upper lithophysae-bearing zone of the crystal-poor member of the Tiva Canyon Tuff (after Barton et al., 1993). (A) Pavement P100. (B) Pavement P200. (C) Pavement P300. Pavement locations in Figure 2A. Thick lines—tube-bearing joints; thin lines—other fractures; dashed line—perimeter of mapped pavement; medium gray regions—abundant small fracture traces; dot-patterned regions—fracture faces; arrowhead symbol—north direction.**

et al., 1995). Devitrification and vapor-phase mineralization likely continue after compaction ceases, but probably also stop about a century after emplacement (e.g., Keith, 1991; Riehle et al., 1995). Joints that are post–lithophysae formation but synmineralization will likely cut or terminate in lithophysae and also show effects of devitrification and vapor-phase mineralization in adjacent rock walls. Finally, joints may form through cooling-induced contraction of the tuff to ambient temperatures (e.g., DeGraff and Aydin, 1987), which can occur more than a century after deposition without associated mineralization or alteration.

## JOINT GEOMETRY AND ORIGIN

Since being identified as a potential site for the permanent disposal of high-level nuclear waste, Yucca Mountain has been a focus of several fracture analyses. Fractures have been investigated at the surface (e.g., Morgan, 1984; Barton et al., 1984, 1993; Barton and Larsen, 1985; Sweetkind et al., 1995a, 1995b; Throckmorton and Verbeek, 1995), in new tunnels (e.g., Albin et al., 1997; Eatman et al., 1997; Mongano et al., 1999), and in boreholes (e.g., Carr, 1992). The early surface analyses used the then-novel approach of clearing pavements of ~200 to 250 $m^2$ (Fig. 3) to investigate fractures as two-dimensional networks (e.g., Barton et al., 1993) rather than rely on scan-line or anecdotal station data (Hancock, 1985; La Pointe and Hudson, 1985). The tunnel data set consists of a rigorously collected scan line that sampled 15 fracture attributes and a periphery map of the tunnel walls for fracture traces greater than 1 m in length. It is the largest and most thorough data set concerning fractures at Yucca Mountain (CRWMS M and O, 2000, and references therein). Tunnels sample almost the entire Paintbrush Group, whereas surface data

Downloaded from gsabulletin.gsapubs.org on November 12, 2010


are mostly from the Tiva Canyon Tuff, which dominates the outcrop on the crest and eastern flank of Yucca Mountain.

The consensus of the surface investigations, which was also applied to the subsurface work, was that the natural fractures at Yucca Mountain include joints that have three origins with distinct relative ages determined from abutting relationships (Hancock, 1985; Sweetkind and Williams-Stroud, 1996). Volcanic cooling joints are the oldest, largest, most planar natural joints, and they commonly have tube structures along their walls (Barton et al., 1984; Sweetkind and Williams-Stroud, 1996; Buesch et al., 1999) (Figs. 1A, 1B, 1C, 4). Next, tectonic joints, which postdate cooling and have geometries resulting from stress fields controlled by regional stress conditions, abut the cooling joints, are planar to curviplanar, are larger when fewer older cooling joints are present, and are smooth to rough. Unloading joints, which are youngest and formed near the present ground surface in response to surficial unloading by erosion, have hackly, irregular surfaces and are typically subparallel to the ground surface.

A subset of the ''cooling'' joints as defined by previous workers are the focus of this study. We use the descriptive term ''tube-bearing'' to refer to these joints, because they have a unique geometry and because an origin as contractional fractures formed during cooling is questioned here. To the best of our knowledge after an extensive literature search, tube-bearing joints have only been reported in ignimbrite deposits at Yucca Mountain, Nevada. If, as discussed subsequently, these joints formed prior to lithophysae formation, then the apparent rarity of tube-bearing joints in welded lithophysae-bearing ignimbrites may reflect the difficulty of forming brittle fractures before lithophysae formation in the first few days after pyroclastic flow emplacement.

Across much of Yucca Mountain, tube-bearing joints occur in two subvertical orthogonal sets that are normal to flow foliation and in a locally developed third set that is subhorizontal and parallel to flow layering. This third set is rare, and its joints tend to have curviplanar rather than planar geometries, which could simply result from vertical dilation during cooling and degassing. Joints in the third set are not the focus of this study (Throckmorton and Verbeek, 1995; Sweetkind and Williams-Stroud, 1996). In the central block of Yucca Mountain, the orthogonal sets typically strike northeast (Figs. 3A, 1C, 5) and northwest (Figs. 1D, 4C, 5). The relative age of the two orthogonal sets is not well constrained from field data, as only a few abutting relationships are found (Figs. 1D, 3). For example, at pavements P100 and P300 (Fig. 3), more northwest-striking tube-bearing joints terminate against northeast-striking joints than vice versa, and almost all northeast-striking joints that terminate against northwest-striking joints are less than 2 m in trace length, which is much shorter than the typical size of these joint traces. Although neither geometric aspect is conclusive, the joints support an interpretation in which the majority of the northeast-striking, tube-bearing joints are older than the northwest-striking ones.

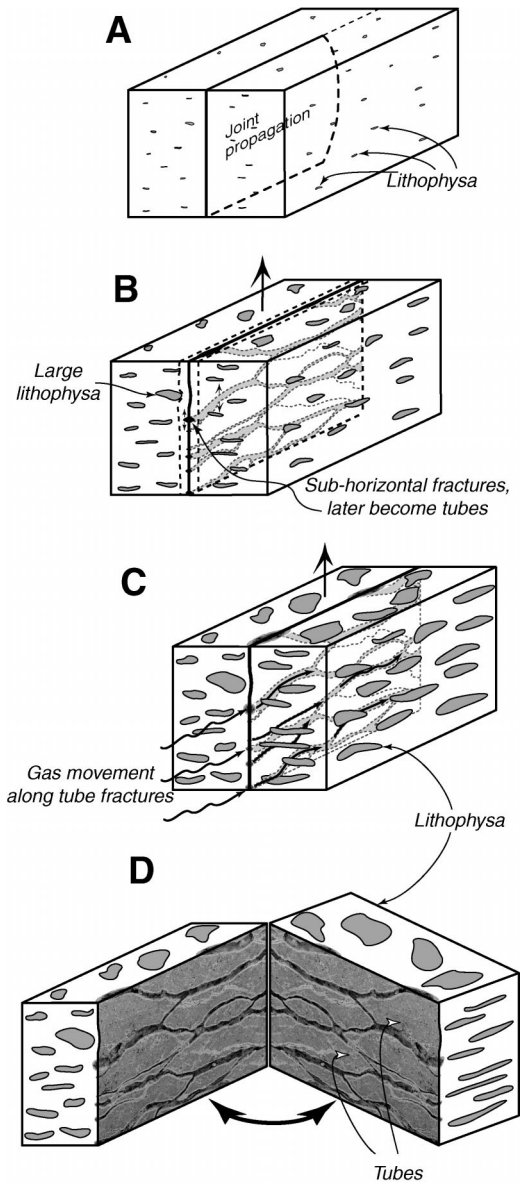


**Figure 4. Sequence of formation of cooling joints with tubes. (A) Contractional joint surface propagates through rock prior to the formation of lithophysae, so no joints terminate or cut lithophysae. (B) Cooling joint causes formation of adjacent brittle zone. As the rock expands vertically with the formation of lithophysae, subhorizontal, tube-like fractures develop within the brittle zone. Also, large lithophysae deflect joints. (C) Continued degassing of the rock utilizes these tubes for gas flow (arrows show gas flow). (D) An expanded view of a cooling joint shows that the two sides are mirror images of each other.**

When considering the geometry of the orthogonal system at the scale of Yucca Mountain, based on anecdotal field observations, some workers have suggested that the two sets form a rectilinear pattern of joint swarms or clusters with swarm widths of 3–5 m and spacings between swarms of 150–200 m (Barton et al., 1993; Sweetkind and Williams-

Downloaded from gsabulletin.gsapubs.org on November 12, 2010


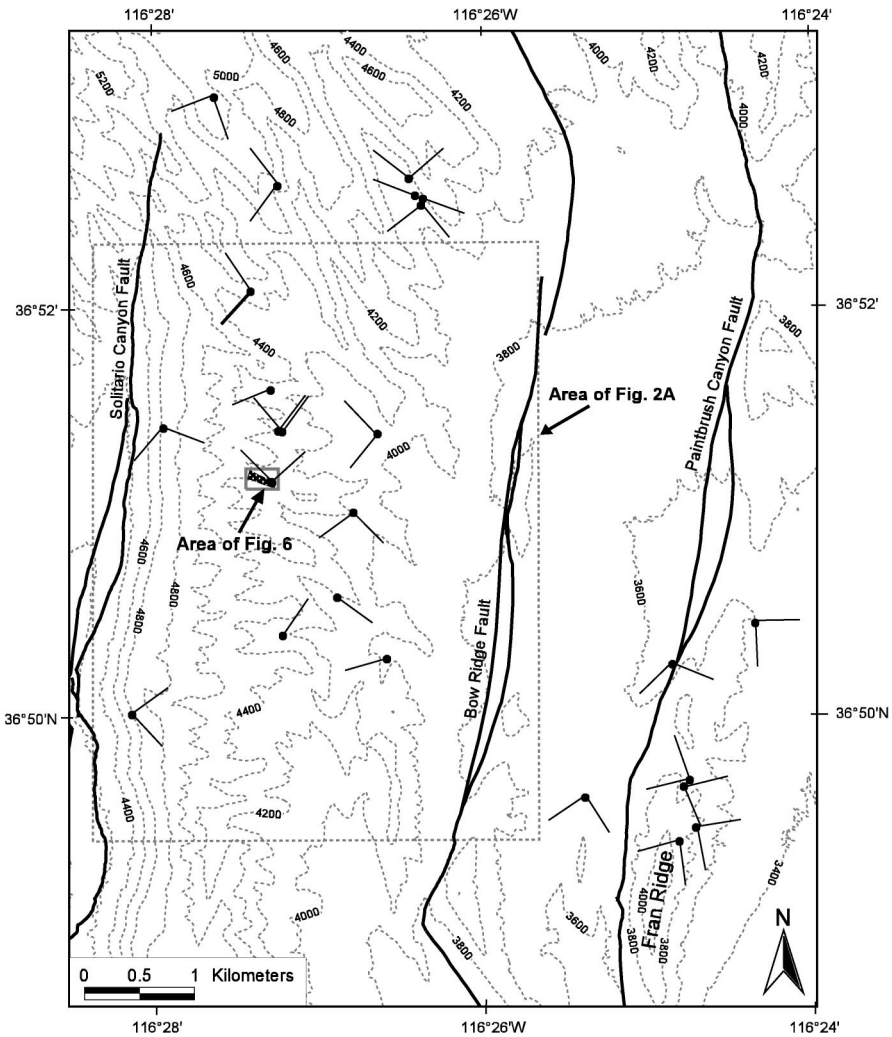


**Figure 5. Map of Yucca Mountain to Fran Ridge (see Fig. 1B) region showing strikes of orthogonal tube-bearing joints (modified from Throckmorton and Verbeek, 1995) and the locations of Figures 2A and 6. Dots on joint-trend tips are station locations.**

Stroud, 1996). The present study attempts to resolve the importance of the orthogonal sets of tube-bearing joints in the overall fracture network by considering their orientations over areas of thousands of square meters as opposed to hundreds of square meters.

## Timing of Tube-Bearing Joints and Volcanogenic Features

Tube-bearing joints at Yucca Mountain have two characteristics that we interpret to indicate that joint formation preceded lithophysae formation. First, the fact that some joint walls within ~1 cm of a lithophysa show outward deformation due to inflation of the lithophysa indicates that the walls are older (Figs. 1E, 1F). Second, tube-bearing joints seldom intersect lithophysae, although lithophysae are common and the tube-bearing joints are large (Figs. 1A, 1C, 1D). If joint propagation occurred in the presence of lithophysae, intersections and terminations with lithophysae should occur (Barton et al., 1993; Buesch et al., 1996), partly because some joints should have propagated toward existing lithophysae in response to local stress perturbations around the expanding void (Kirsch, 1898; Lachenbruch, 1962).

Tube-bearing joints also have two features that we interpret to indicate that joint formation preceded tube formation. First, tubes are found only on joint faces and not in the rock mass, where lithophysae are present. Second, some tubes pass through joint intersections, which indicates that these intersections are older.

The millimeter- to centimeter-diameter tubes form anastomosing networks, which isolate areas of joint planes (Figs. 1B, 1D, 1G). Area edges match across tube walls, indicating that the tubes dilated joint faces. Restoration to a predeformation configuration (Fig. 1G) shows that tubes produced at least 15% vertical dilation of the joint face, accompanied by a few degrees of local rotation for some areas. This magnitude of vertical dilation is consistent with vertical expansion in the ignimbrite unit of 16% to 22% due to lithophysae formation described by Barton et al. (1993) (Fig. 4). Thus, the tubes are degassing structures (Barton et al., 1993) that formed coevally with the lithophysae in response to vertical inflation of the ignimbrite. Because the tube-bearing joints are older than both the lithophysae and the tubes and because gas pressure must have exceeded lithostatic pressure for their inflation, the time frame for their formation bounds the timing of joint development in a lithophysae-free ignimbrite. Thus, joint formation likely occurred within a month of tuff emplacement (i.e., Riehle et al., 1995).

Abundant vapor-phase silicates line the tube interiors, and devitrification selvages commonly extend for half a tube diameter into the ignimbrite matrix. In contrast, joint planes between tubes show only minor vapor-phase mineralization and very limited amounts of devitrification into the joint walls (Fig. 1G). Thus, hot gases flushed through the tubes rather than along the joint faces, leaving most of the vapor-phase precipitation products on the tube walls. Further cooling permitted escape of the less saturated gas vertically along the joint.

## Structural Geometry of Tube-Bearing Joints

A sample area of 20,787 $m^2$ with ~15% exposure was examined on Live Yucca Ridge at Yucca Mountain to characterize the contribution of the orthogonal joint system to the total fracture network (Figs. 5, 6). Subhorizontal tube-bearing joints are not exposed in this area, so their geometry is not considered.

Both fracture traces and limits of exposed rocks were mapped to consider the influence of the distribution and quantity of rock exposure on trace distribution. The sample area is about two orders of magnitude larger than that used for the cleared pavements, such as P100 (214 $m^2$; Fig. 3A), which is within the new sample area (Fig. 6).

We used a real-time kinematic differential GPS (DGPS) (Novatel) with resolution of ±2 cm horizontal and ±10 cm vertical (2σ error) to map the topography of Live Yucca Ridge and to create a fracture trace map. Fracture

Downloaded from gsabulletin.gsapubs.org on November 12, 2010


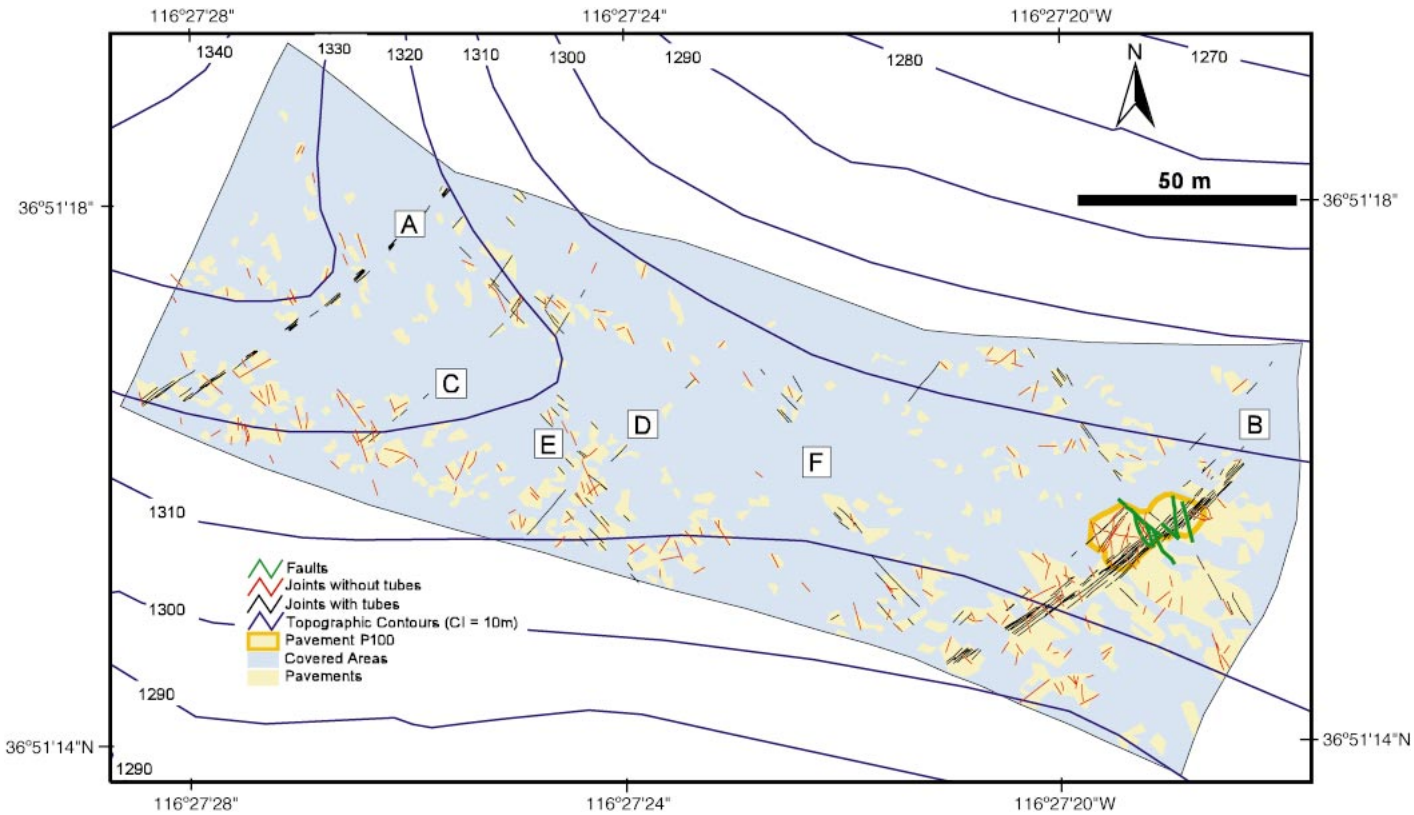


**Figure 6. Map of Live Yucca Ridge, Yucca Mountain, showing joint traces, faults, and rock exposures (pavements). Topographic contour interval is 10 m, and location grid is the UTM, Zone 11, NAD27 system. Letters in rectangles are locations referred to in the text.**

positions were mapped by using the GPS data collector's ''feature tagging'' option, where the position is ''tagged'' with a user-defined alphanumeric identifier. Fractures were tagged at their visible ends and at several points in between if they exceeded a few meters in length. Fractures were sequentially numbered and designated as either bearing or lacking tubes. In addition, fracture orientations were measured with a Brunton compass and input into the data collector. The tagged data points were then connected in a GIS (Arcview) to create a trace map of the fractures. Other field observations were measured and recorded with compasses, field notebooks, and cameras.

To facilitate useful, but efficient data collection over such a large sample area, the minimum recorded trace length of the fractures (i.e., cutoff length) was 2 m, and the minimum exposed area mapped was approximately equal to a circle with a diameter of 2 m. The truncation limit is an order of magnitude larger than the 0.2 m limit used to survey fracture traces on pavements such as P100 (Barton et al., 1993). We used a larger truncation limit because previous work and our reconnaissance mapping indicated that (1) tube-bearing joints dominantly have trace lengths greater than 2 m, (2) previous pavement work (Barton et al., 1993) provided sample sets for the geometry of smaller fractures, and (3) previous investigations at Yucca Mountain documented the tremendous increase in time necessary to accurately document the patterns for trace lengths of <1 m (Sweetkind and Williams-Stroud, 1996).

P100 and the related swarm of northeast-striking tube-bearing joints are in a relatively well exposed part of the ridge. However, visual inspection of the mapped locations of tube-bearing joints shows that their abundance does not correlate to areas of best exposure (Fig. 6).

The true maximum length of tube-bearing joints is difficult to ascertain because their trace lengths are so long that they exceed the dimensions of even the largest exposures and hence are censored (joint tips are not exposed) (Epstein, 1954; Priest, 1993; Mauldon et al., 2001). In a few cases, joints were traced by using small discontinuous exposures between 2-m-diameter exposures to partly overcome the effects of censoring and determine maximum trace length. These traces are visible as black lines that are mostly not contained in regions of exposure in Figure 6. Even with these efforts, true fracture tips were seldom found for tube-bearing joints, and we are restricted to saying that many tube-bearing joints have trace lengths exceeding 10 to 15 m.

The two sets of tube-bearing joints have different trace distribution patterns. Northeast-trending traces are generally longer (apparent mean trace length of 4.1 m vs. 3.6 m) and are either grouped in narrow swarms (locations A and B, Fig. 6) or occur as a few joints in near alignment (locations C and D, Fig. 6). In contrast, northwest-striking tube-bearing joints occur in wider swarms and have traces that are more typically en echelon rather than collinear (locations E and F, Fig. 6). Also, northwest-striking joints are less numerous (67 vs. 126) than northeast-striking joints (locations A and B, Figs. 6 and 7A).

The two sets of joint swarms form an approximately rectilinear network of traces (Fig. 6), as described by Barton et al. (1993). The orthogonal distance between the two well-developed northeast-striking joint swarms is ~150 m (Barton et al., 1993). This value is probably an overestimate of the swarm spacing, because between the two well-developed northeast-striking swarms are two poorly developed swarms, particularly around location C in Figure 6, yielding a minimum swarm spacing of ~50 m for the northeast-striking

Downloaded from gsabulletin.gsapubs.org on November 12, 2010


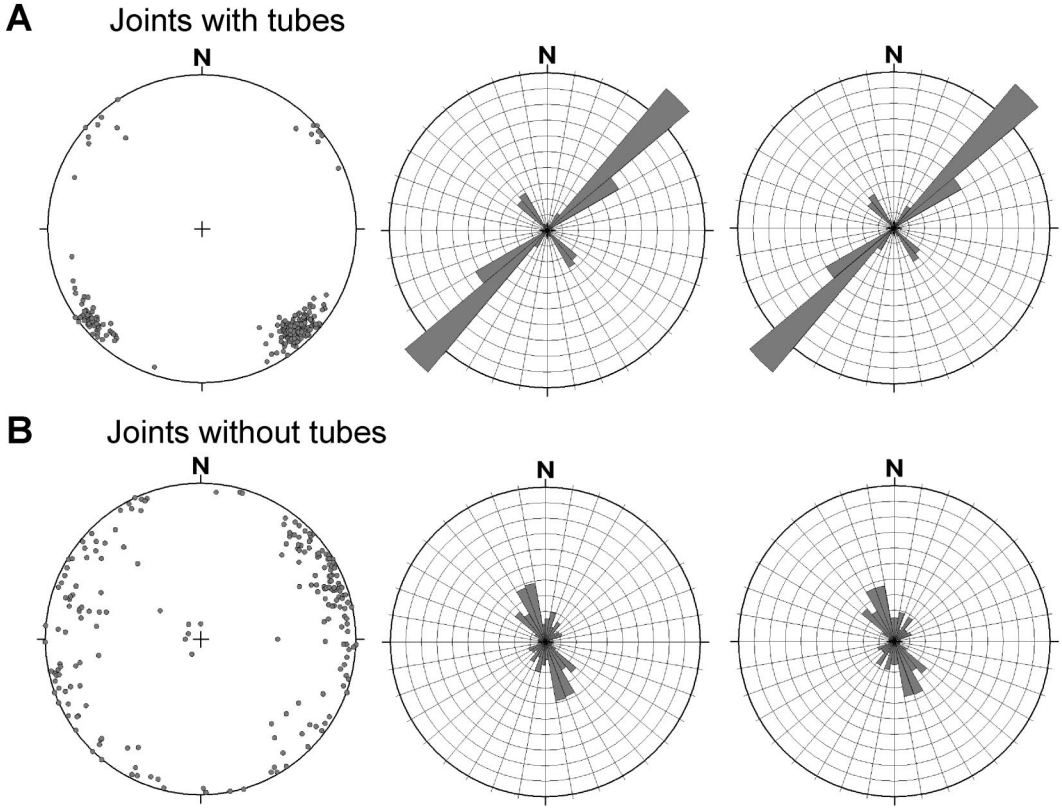


**Figure 7. Orientation data for joints on Live Yucca Ridge. Left column: Lower-hemisphere, equal-area plots of poles to joints. Middle column: Unweighted rose diagrams of joint traces. Plot radius = 20%. Right column: Length-weighted rose diagrams of joint traces. Plot radius = 20%. (A) Tube-bearing joints; number of joints = 272; cumulative trace length = 1069 m. (B) Joints without tubes; number of joints = 214; cumulative trace length = 737 m.**

set. The northwest-striking swarms also have spacings of ~50 m.

Tube-bearing joints have a greater cumulative trace length with a narrower orientation range than joints without tubes (Figs. 6, 7). Even with censoring, field observations demonstrate that the traces of tube-bearing joints, particularly northeast-striking ones, are longer than the traces of joints without tubes and that tube-bearing joints are more numerous. Thus, the swarms of tube-bearing joints provide a rectilinear framework to the fracture network, whereas joints without tubes enhance fracture-network connectivity.

### Fumarolic Association for Tube-Bearing Joints

Many ignimbrite deposits have early-formed joints (e.g., Sheridan, 1970; Hildreth, 1983; Keith, 1991), and near-orthogonal joints in ignimbrites have previously been recognized (Keith, 1991). Early-formed joints in the Valley of Ten Thousand Smokes and Bishop Tuff (Hildreth, 1983; Keith, 1991; Sheridan, 1970) are associated with fumarolic degassing and have obvious gas-escape features such as mineralized ridges at the top of the deposit and vapor-phase alteration of joint walls. These fumarolic joints have not been reported with tubes, but neither have they been investigated in units with lithophysae (e.g., Sheridan, 1970; Hildreth, 1983; Keith, 1991). Fumarolic joints in these ignimbrite deposits occur along ridges that are underlain by single long joints or narrow swarms of joints (see Fig. 3A in Sheridan, 1970), which is consistent with the geometry of the tube-bearing joints at Yucca Mountain. Fumarolic joints provide the vertical pathways for gas escape during ignimbrite compaction and welding, and their host ridges have lengths from as little as tens of meters to greater than 1 km. As a result, the underlying swarms of fumarolic joints would have the same lateral persistence as the ridges. Fumarolic joints formed during ridge construction are driven both by the thermoelastic contraction expected for simple cooling joints (Engelder and Fischer, 1996) and by elevated fluid pressure (Secor, 1968) due to degassing. Given that tube-bearing joints at Yucca Mountain are geometrically similar to fumarolic joints, are the oldest joints, and formed in a lithophysae-free matrix, we interpret them to have been very early gas-escape pathways that may have served as the plumbing system for fumaroles at the surface.

### Possible Stress Sources for Developing Subvertical Tube-Bearing Joints

Because the Tiva Canyon Tuff was deposited in a region undergoing east-west extension (Zoback et al., 1981; Sawyer et al., 1994; Morris et al., 1996), and under the assumption that the orthogonal joints are mode I extension fractures with wall-normal displacements, they might be expected to strike north and east. However, across much of the Yucca Mountain region, the two tube-bearing sets strike northeast and northwest (Figs. 3, 5, 6, 7). Thus, at least one additional stress component other than the remote regional stresses must have operated to perturb the stress field from the regional stress state. Such stress perturbation might result from crustal subsidence during caldera formation or from active normal faulting during or just after ignimbrite deposition.

During ignimbrite cooling, temperature gra-

Downloaded from gsabulletin.gsapubs.org on November 12, 2010


dients are greater vertically than horizontally. Although the formation of the subvertical joints could not be driven by tension related to the vertical temperature gradient, their formation could be partly explained by horizontal temperature gradients (Lachenbruch, 1962), although one might not expect them to be uniform in direction across a region. As an aside, the vertical temperature gradient, and consequent differential thermal contraction, may help explain the stress conditions for the formation of the rare subhorizontal tube-bearing joints, although gas pressure may have had a role as well.

Another cooling-related effect is differential compaction where thicker ignimbrite deposits remain hotter for longer periods and compact more than thin deposits because of their higher total heat capacity. This variation in thickness creates a lateral stress gradient. For example, one set of fumarolic ridges in a system of orthogonal ridges in the Valley of Ten Thousand Smokes, Alaska, was interpreted to form in response to differential compaction during cooling of the ignimbrite (Keith, 1991). As the ignimbrite deposit cooled, ignimbrite in the valley center compacted more than that at the margins, creating tensional fissures parallel to these margins. In another example for the general case of a simple basin, Sheridan (1970) proposed that vertical joint formation could be driven by differential compaction between the depocenter (i.e., thick deposits, more compaction) and the basin margins (i.e., thin deposits, less compaction). For the Tiva Canyon Tuff at Yucca Mountain, if the depocenter of a northwest-trending basin existed just to the north of the study area (Fridrich, 1999), the steepest compaction and temperature gradient would be along the short axis of the basin toward the depocenter. Thus, the greatest cooling-generated tension would be oriented northeast-southwest and would possibly generate northwest-striking vertical joints.

The eruption that formed the Tiva Canyon Tuff involved ejection of ~1000 $km^3$ of magma and collapse of the Claim Canyon caldera ~7 km north of the present study area (Fig. 2B; Byers et al., 1976; Sawyer et al., 1994; Potter et al., 2002). Such a collapse would have perturbed the regional stress field directly and likely would have triggered movement on nearby normal faults (e.g., Nostro et al., 1998). For example, volcanic eruptions with less than 1% of this volume are interpreted to trigger earthquakes on normal faults in regions with active extension (e.g., Abe, 1992; Nostro et al., 1998, and references cited within). The interval between the two events is typically 1 to 10 yr, but could be much shorter for a large event.

The major normal faults in the Yucca Mountain region were active within the 100,000 yr interval before and during the million years after deposition of the Tiva Canyon Tuff. The fault activity was in response to regional extension in the central Basin and Range province and is documented by thickness changes in tuffs adjacent to major faults (Christiansen et al., 1977; Sawyer et al., 1994; Day et al., 1998a; Fridrich, 1999). Thus, regional tectonic stresses with or without perturbation from caldera formation, plus the increased lithostatic load from deposition of the Tiva Canyon Tuff, could have reasonably triggered normal faulting during ignimbrite cooling. If one or more of the normal faults in the area slipped, the regional stress field would be locally perturbed, which could explain an orthogonal joint geometry that did not match horizontal stress directions for the regional stress field alone (e.g., Crider and Pollard, 1998; Kattenhorn et al., 2000).

Ideally, one would like to quantitatively test these possibilities individually and together. However, lack of data, limited understanding of the material behavior of complexly cooling ignimbrites, and a lack of robustness of current mechanical models to handle some of these uncertainties preclude rigorous testing. The role of differential compaction and thermal gradients cannot be tested, owing to the paucity of data about depositional thickness, possible basin geometry, and lateral temperature variations during emplacement and cooling. Analytical models have been developed for modeling stress perturbation around small-volume magma systems, but not for stress-field perturbation effects from very large volume (~1000 $km^3$) eruptions. Nevertheless, the available data for the orientation and distribution of tube-bearing joints, for normal-fault geometry, and for possible regional stress conditions during the Miocene at Yucca Mountain do allow us to test whether interacting normal faults could have locally perturbed the regional stress field sufficiently to lead to the formation of the swarms of fumarolic tube-bearing joints.

## NORMAL FAULTING AND PERTURBATION OF THE REGIONAL STRESS FIELD

We use a numerical model to test the following proposition: active faulting could have locally perturbed the stress field to produce a joint system with strikes different from expected in the Miocene regional stress field. The tool we use is Poly3D (Thomas, 1993), a numerical code based on a three-dimensional boundary-element method. Supplemental description of the numerical modeling procedure and results are available.[1] The code solves the elastostatic equations for the stress and deformation fields around composite surfaces of displacement discontinuity (Crouch and Starfield, 1990; Comninou and Dundurs, 1975; Jeyakumaran et al., 1992). Poly3D has been benchmarked against two-dimensional analytical solutions and shown to give results accurate to within a few percent (Crider and Pollard, 1998). Advantages to using the boundary-element method are that it is computationally efficient and that we can specify discontinuities, such as faults, of any shape. A disadvantage is that we are limited to testing the deformation of a homogeneous, isotropic, and isothermal medium.

Poly3D has been extensively tested and applied in the study of the mechanics of normal faulting, including fault interaction related to slip distribution (e.g., Willemse et al., 1996) and linkage (e.g., Crider, 2001); stress-triggering of earthquakes (e.g., Crider et al., 2001); and, most relevant to this work, fault control of the orientation of secondary structures, including joints (e.g., Kattenhorn et al., 2000) and faults (Maerten et al., 2002). We refer the reader to these works and to Thomas (1993) for further details about the model.

We modeled the fault system in the vicinity of the field study area with a simplified geometry and very simple material properties. Our goal was to evaluate the hypothesis that fault slip during cooling of the Tiva Canyon Tuff may have influenced the orientation of the tube-bearing joints, not to reproduce the complete natural system.

### Model Configuration

We modeled the four major faults that occur near the field study area: the Solitario Canyon fault, the Iron Ridge fault, the Paintbrush Canyon fault, and the southern segments of the Bow Ridge fault (Fig. 8). The fault traces have been mapped by numerous workers (e.g., Scott and Bonk, 1984; Day et al., 1998a; Potter et al., 2002). The fault geometry at depth is not as well constrained, but is reasonably interpreted to be steeply dipping to a depth of 4 km before becoming listric (Young et al., 1992; Ferrill et al., 1996b). We modeled only those segments with significant present-day topographic expression, and thus we do not

[1]GSA Data Repository item 2003168, supplemental description of the numerical modeling procedure and results, is available on the Web at http://www.geosociety.org/pubs/ft2003.htm. Requests may also be sent to editing@geosociety.org.

Downloaded from gsabulletin.gsapubs.org on November 12, 2010


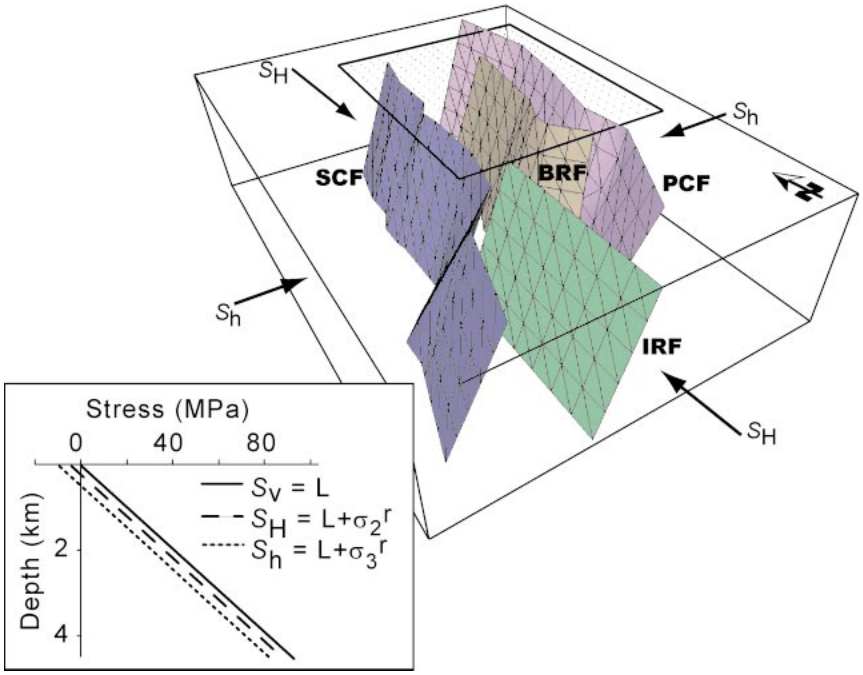


**Figure 8. Perspective view of model fault geometry. SCF—Solitario Canyon fault (blue), IRF—Iron Ridge fault (green), BRF—Bow Ridge fault (brown), PCF—Paintbrush Canyon fault (purple). Arrows indicate the direction of maximum ($S_H$) and minimum ($S_h$) horizontal stresses. Surface traces of the faults are coincident with the free surface of the model elastic half-space. Half-space is semi-infinite; bounding box is shown to illustrate perspective only. Dimensions of the bounding box are 14 km × 19 km × 5 km (east, north, depth). Rectangle at surface shows approximate area of Figures 5 and 9A. Dots show calculation grid for principal stresses. Inset: Stress vs. depth plot illustrating model's boundary conditions. The vertical principal stress ($S_V$) is equal to the lithostatic load ($L$). Horizontal principal stresses deviate from lithostatic by amounts equal to the applied remote stresses ($\sigma_2^r$ and $\sigma_3^r$). For the results shown in Figure 9, $\sigma_2^r = -10$ MPa and $\sigma_3^r = -8$ MPa.**

include the east-dipping segment of the Bow Ridge fault where it crosses Yucca Wash. The modeled fault geometry (Figs. 8 and 9A) uses simplified fault traces from within the region covered by Figure 5 and from Day et al. (1998a) for the area outside Figure 5. The modeled faults dip west at 70° to a depth greater than 4 km. Because our interest is in very near surface phenomena, the deep, listric parts of the faults were not included. Smaller intrablock faults were also not included, so that we could focus on the generalized effects of stress perturbation by the major structures.

For the purposes of this analysis, we assumed that the Tiva Canyon Tuff is mechanically coupled to the rocks below and that deformation is influenced by the stress state of the entire rock volume containing the modeled faults. The model faults are embedded in a semi-infinite elastic half-space with standard crustal rheology (Poisson ratio = 0.25, shear modulus = 30 GPa). Although we expect the cooling Tiva Canyon Tuff to have been significantly less stiff, it represents only a small volume of the modeled crustal section. Thus, we choose rheology appropriate to the larger volume. Model trials with order-of-magnitude variation in shear modulus (3 GPa to 100 GPa) show no difference in the resulting orientations of local stress directions (see footnote 1). The faults intersect the free surface of the half-space and are allowed to slip freely (no friction). Thus, modeled faults will slip in response to any magnitude of differential stress, and the stress drop across slipped faults is complete.

Although it is not possible to obtain direct measurements of the stress state in the Miocene, we assumed that deformation occurred in a normal-faulting stress regime with maximum principal compressive stress vertical ($S_V$), intermediate principal stress horizontal and north-south ($S_H$), and minimum principal compressive stress horizontal and east-west ($S_h$). This assumption is consistent with geologic estimates of the Miocene stress state, as interpreted by Zoback et al. (1981). Modern values for the principal stresses provide a framework for values used in the model. Ferrill et al. (1999b) determined fluid-pressure–corrected principal-stress values at 1 km depth on the basis of stress measurements by Stock et al. (1985). These are $S_V$ = 21 MPa (approximately lithostatic), $S_H$ = 17 MPa (4 MPa less than lithostatic), and $S_h$ = 11 MPa (10 MPa less than lithostatic). By using the Miocene stress directions and the modern values as a guide, we applied to the model a linearly increasing lithostatic stress ($L$, equivalent to the weight of overlying rock) acting in all directions ($S_V = L$). To drive deformation, we reduced the horizontal stress in the north-south and east-west directions (Fig. 8 inset), as is observed in the modern stress data. Because we were testing the orientation and not the magnitude of Miocene stresses, the magnitude of the boundary stresses is not as important as the ratios among them. Several variations were tested. We report one here, and others are available to the reader (see footnote 1).

## Model Results and Interpretation

With the boundary conditions just described, the modeled faults slip simultaneously, with maximum dip slip at the free surface and approximately at the center of the fault trace (see footnote 1). Slip distribution along each fault is approximately elliptical, modified by interaction among the faults. The faults also show small components of strike slip where the strike of segments deviates from north. For $S_h$ equivalent to modern values, the mean dip slip on the faults is less than 1 m. The modeled situation corresponds to a cluster of moderate-sized ($M_w$ = 5 to 6) earthquakes, such as is common in western North America, e.g., the 1993 Klamath Falls, Oregon, earthquakes (Braunmiller et al., 1995), the Ridgecrest, California, sequence (Hauksson et al., 1995), or the much larger Dixie Valley–Fairview Peak, Nevada, sequence (Doser, 1986).

In Figure 9, we present results for remote driving stresses $S_h = L - 10$ MPa (east-west) and $S_H = L - 8$ MPa (north-south). The results are calculated at a preerosion depth of 100 m. Vertical tensile fractures are expected to form perpendicular to the local least horizontal stress. Outside the faulted region, a dominant north-south fracture pattern perpendicular to the regional $S_h$ is predicted (see footnote 1). Near the faults, local perturbation of the principal stress orientations and consequent rotation of predicted fracture orientations is observed. Figure 9 shows local orientations for $S_h$ and predicted fracture orientations in the vicinity of Live Yucca Ridge. These compare favorably to the ob-

Downloaded from gsabulletin.gsapubs.org on November 12, 2010


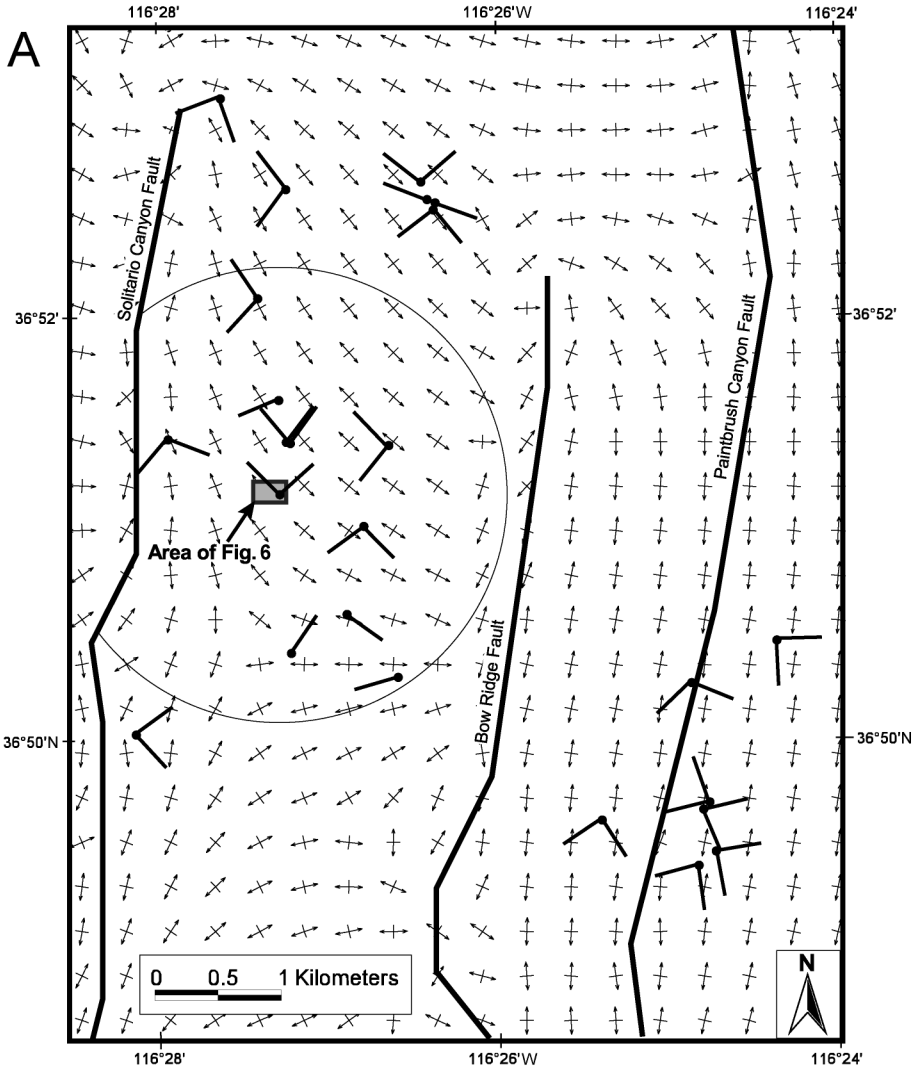


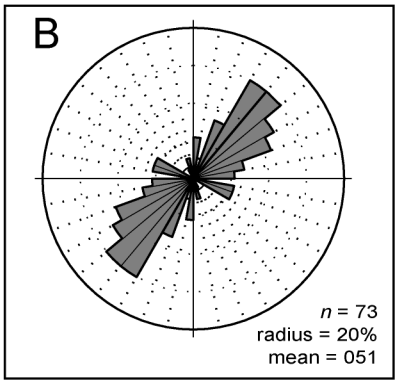


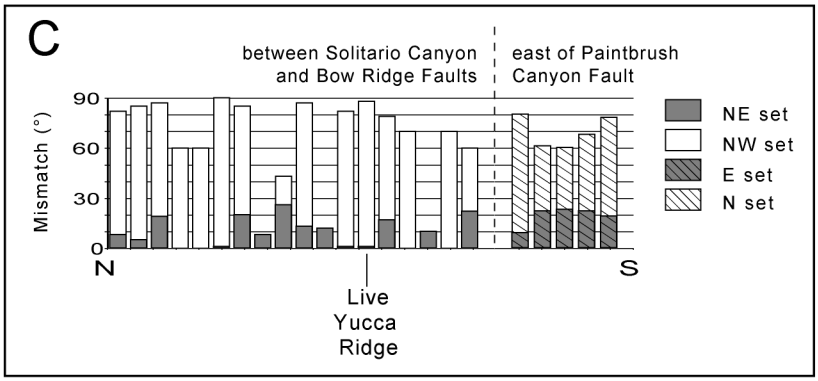


**Figure 9. Modeled stress trajectories and predicted joint orientations compared to observed structures. (A) Modeled fault traces and stress trajectories overlaid on joint orientations from Throckmorton and Verbeek (1995). Compare to Figure 5. Arrows show the directions of $S_h$, and short lines show the corresponding predicted joint orientations. Other symbols as in Figure 5. Outside the faulted region, east-west and north-south joint orientations are predicted. In the block between the Solitario and Bow Ridge faults, joint orientations are deflected to the northeast, in correspondence with field observations. Arc shows 2 km radius from Live Yucca Ridge and encircles modeled joint orientations plotted in B. (B) Rose diagram of predicted first-formed joint orientations within 2 km of Live Yucca Ridge. Compare to Figure 7. (C) Angular mismatch between strike of observed joints and predicted joint orientations. In the vicinity of Live Yucca Ridge, average mismatch between the modeled joints and observed northeast-striking set is 12°. Average mismatch between the modeled and observed northwest-striking set is 75°. East of Paintbrush Canyon fault, the average mismatch between the model and observations is 19° for east-striking joints and 69° for north-striking joints.**

Downloaded from gsabulletin.gsapubs.org on November 12, 2010


served orientations of the northeast-striking tube-bearing joints. Within 2 km of Live Yucca Ridge, the model predicts joint strike primarily between 020° and 070°, with a mean strike at 051° and a mode at ~040° (Fig. 9B). These predicted values compare favorably with observed orientations of tube-bearing joints. In the crustal block between the Solitario Canyon and Bow Ridge faults, predicted joints are on average within 12° of the observed northeast-striking set and 75° divergent from the northwest-striking set. At Live Yucca Ridge, the mismatch is 1° and 88°. In the footwall of the Paintbrush Canyon fault, north- and east-striking joints are observed (Throckmorton and Verbeek, 1995), and the model predicts similar joint orientations.

Our model results show that slip on faults can generate local stress perturbations that are consistent with the orientations of northeast-striking joints observed at Yucca Mountain. We emphasize that the model was not designed to be an inversion of the joint-orientation data, nor was it tuned for best-fit results. We use the model to test the proposition that fault slip, driven by geologically reasonable boundary conditions, could have influenced the local joint orientations observed to be different from those expected to be produced by the Miocene regional stress field. The close correspondence between this simple mechanical model and the observed northeast-striking joints suggests that active faulting synchronous with the emplacement of the Tiva Canyon Tuff is a plausible mechanism for controlling the orientation of tube-bearing joints within the ignimbrite. Further, the results suggest that the northeast-striking joints were formed before the northwest-striking set, as the modeled stress trajectories produce northeast-striking joints without the influence of the northwest-striking set.

## FORMATION OF THE NORTHWEST-STRIKING JOINT SWARMS

If it is assumed that the northeast-striking set of tube-bearing joints in the Tiva Canyon Tuff was formed during volcanic degassing and active normal faulting, what was the mechanism that formed the second orthogonal set with the necessary 90° switch of the horizontal stress directions? The likely possibilities are a regional-scale switch of stress directions, changes in displacement behavior of the normal faults, and more local-scale switching due to formation of the first-formed northeast-striking joints. Any of these mechanisms could have been aided by differential compaction in the postulated northwest-trending basin.

If a regional-scale switch is considered, the central Basin and Range in which Yucca Mountain lies, underwent east-west extension prior to 10 Ma (Zoback et al., 1981). Previous work (Zoback et al., 1981; Wernicke, 1992; Axen et al., 1993) does not indicate that a change occurred in regional principal strain directions and, hence, regional principal stress directions during this east-west extension. Consequently, we discount the possibility of a regional-scale switch of tectonic stresses.

Considering displacement behavior on the normal faults, horizontal stress directions might switch if fault-slip directions changed significantly or if different faults or parts of faults slipped sequentially. We cannot completely discount this possibility, although diagnostic evidence for these scenarios is lacking for the joint system under investigation.

The possibility of a locally controlled switch due to an additional perturbation of the stress field by the formation of the northeast-striking joints remains. The fact that the northeast-striking joint swarms are better developed than the northwest-striking swarms in terms of joint size and abundance within swarms provides a geometric support for this possibility. The better development of the older set is a typical feature of orthogonal joint systems formed by local stress release (Hancock, 1985; Caputo, 1995; Bai et al., 2002).

The case for local control of the switch of the stress directions is analogous to the formation of strata-bound layer-normal joints forming in response to remote tension (Hobbs, 1967; Gross et al., 1995). In this case, joint formation perturbs the stress field by causing a stress drop or shadow. Recent work by Bai et al. (2001) shows that when joint spacing of the older joint set is <1.7 times the thickness of the layer containing the joints and when $S_h/S_H > 0.2$, the horizontal stress directions in the rock mass between the first-formed joints switch. Given an interpreted penetration depth for the northeast-striking joints of 20 to 30 m, which is the thickness of the upper lithophysae-bearing zone, and a swarm spacing of ~50 m, the spacing to thickness ratio in the Tiva Canyon Tuff is 2.5 to 1.6, which is about the critical threshold of 1.7 for stress switching when the ratio of horizontal stresses is >0.2, which seems likely in this case, on the basis of the likely stress conditions for fault slip and stress formation. Thus, a second perturbation of the stress field in the vicinity of Live Yucca Ridge by the formation of the swarms of northeast-striking tube-bearing joints is a possible mechanism for rotating the horizontal stress directions to allow the formation of northwest-striking joints.

Care should be taken in applying this analogy to orthogonal swarm formation at Yucca Mountain. The analogous case is applied to fracture networks of individual joints in brittle rocks with spacings on the order of centimeters to meters, whereas the Yucca Mountain case considers swarms of joints on the scale of tens of meters that developed in a cooling, but hot, ignimbrite with a more complex material behavior. The analogous case relies on uplift and erosion to achieve near-surface conditions for formation of the cross joints, whereas at Yucca Mountain the process occurred quite close to the ground surface after minimal burial. Also, whereas joint formation at Yucca Mountain is partly driven externally by thermoelastic contraction due to cooling, the joint formation is also internally driven by fluid pressure generated by volcanic gases, which differs from the analogy. Still, the analogy does offer an explanation. Numerical modeling has the potential to allow the exploration of the possibility of extrapolating this explanation to the larger-scale case of joint swarms partly driven by internal fluid pressure. In fact, the fluid-driven case may offer an explanation for some cases of joint swarm development, which is a widely recognized phenomenon (e.g., Hancock, 1985; Pollard and Aydin, 1988; Odling et al., 1999).

## DISCUSSION

### Cooling Joints Without Tubes

Cooling joints are ubiquitous features in moderately to densely welded ignimbrite deposits (e.g., Smith, 1960; Ross and Smith, 1961; Cas and Wright, 1987). They form in response to tensional stress induced by thermal contraction during cooling (Lachenbruch, 1962; DeGraff and Aydin, 1987; Engelder and Fischer, 1996) and are not associated with ductile deformation features such as tubes or lithophysae (Enlows, 1955; Ross and Smith, 1961; Sheridan, 1970; Cas and Wright, 1987). Cooling joints are pseudocolumnar, smooth, or curviplanar; lack bleached walls; occur in a variety of orientations; and vary in length from 1 to 15 m. They also occur in ignimbrites with fumarolic joints and terminate against those early-formed joints (e.g., Sheridan, 1970).

By analogy with other welded ignimbrites, abundant cooling joints due to thermoelastic contraction should be expected in the rock volumes between early-formed fumarolic joints at Yucca Mountain (e.g., Sheridan, 1970). Such cooling joints have been recognized by previous workers at Yucca Mountain (Morgan, 1984; Barton et al., 1984, 1993; Barton and Larsen, 1985; Carr, 1992; Sweet-

Downloaded from gsabulletin.gsapubs.org on November 12, 2010


kind et al., 1995a, 1995b; Throckmorton and Verbeek, 1995; Albin et al., 1997; Eatman et al., 1997; Mongano et al., 1999). Thus, the lithophysae-bearing part of the ignimbrite contains two systems of joints with origins related to lithification and cooling of the deposit: the fumarolic tube-bearing joints and the younger cooling joints without tubes formed by thermoelastic contraction.

Distinguishing cooling joints from younger tectonic joints is problematic when only geometric characteristics are used. Previous workers have identified a series of characteristics such as size, planarity, and the smoothness of fracture surfaces to distinguish cooling from tectonic joints. These characteristics do distinguish the relative age of two joint sets without tubes, but they do not conclusively demonstrate that either set is of cooling origin. Fortunately, for subsurface joints and surface joints with limited to absent weathering, cooling joints can be identified by using the different deuteric alteration facies within the Tiva Canyon Tuff (cf. Buesch et al., 1996). Cooling joint attributes, such as fill compositions and bleached rims, should correlate with degree of degassing, welding, and devitrification processes in the rock mass, which are attributes not associated with tectonic joint formation (Sweetkind et al., 2003). If the relative abundance of cooling and tectonic joints in the Tiva Canyon Tuff is deemed important to understanding performance of the proposed repository, the previous assignment of a cooling or tectonic origin to joints on the basis of geometric characteristics would benefit from a careful reexamination of the joints for attributes indicative of ignimbrite cooling.

### Implications for Joint Geometry in Other Lithophysae-Bearing Units at Yucca Mountain

The focus of this paper is on tube-bearing joints in the upper lithophysae-bearing zone of the crystal-poor member of the Tiva Canyon Tuff. The results, however, have direct relevance to joints in other lithophysae-bearing parts of the Tiva Canyon and Topopah Spring Tuffs. The best data set for evaluating the distribution and characteristics of tube-bearing joints within Yucca Mountain is the scan-line and full-periphery mapping data from the ESF and ECRB tunnels (Mongano et al., 1999; CRWMS M and O, 1998, 2000). Tube-bearing joints occur in the Tiva Canyon and Topopah Spring Tuffs sampled in the ESF and ECRB tunnels at Yucca Mountain. These joints more typically have a northwest strike rather than a northeast strike and, in several exposures, occur as closely spaced swarms (CRWMS M and O, 1998, 2000; Mongano et al., 1999). Therefore, these subsurface units contain prelithophysae joints in the vicinity of the proposed repository.

The common understanding of the joints that form after lithophysae in lithophysae-bearing units is that those joints are generally not persistent and have a curviplanar form (Sweetkind and Williams-Stroud, 1996; CRWMS M and O, 1998, 2000; Mongano et al., 1999; Sweetkind et al., 2003). This understanding is quite appropriate for the cooling, tectonic, and unloading joints that postdate lithophysae formation because lithophysae arrest fracture propagation, inhibiting the development of large, throughgoing joints. However, the tube-bearing joints are prelithophysae and have extensive individual and swarm geometry in the upper lithophysae-bearing zone of the Tiva Canyon Tuff (Fig. 6). Tube-bearing joints in the subsurface would be expected to have the same extensive individual and swarm geometries, which would influence the mechanical and hydrologic properties of the lithophysae-bearing rock mass. Whereas much of the lithophysae-bearing rock volume will be populated with discontinuous curviplanar fractures as previously described, locally extensive joint swarms will transect the volume, possibly creating fluid pathways and the potential for significant large joint-bounded blocks. Therefore, when considering the role of joints in a fracture characterization of a lithophysae-bearing unit, a distinction needs to be made between the case of a rock volume with and one without tube-bearing joints.

## CONCLUSIONS

1. The oldest joints in the welded Tiva Canyon Tuff at Yucca Mountain are tube bearing and consist of two orthogonal sets. They were previously interpreted to be related to ignimbrite degassing and dilation during cooling. Given that such processes likely occurred within one month of ignimbrite deposition, we think that the entire orthogonal joint system formed within that time frame.

2. Our proposed interpretation for the formation history of tube-bearing joints is consistent with field data and model results, including *(a)* initial pyroclastic eruption of the Tiva Canyon Tuff and collapse of the Claim Canyon caldera; *(b)* deposition of the ignimbrite over topography that may have included a shallow northwest-trending basin; *(c)* development of a perturbed stress field due to a combination of thermal gradient, differential compaction, caldera collapse, and faulting; *(d)* slip on the Solitario Canyon, Bow Ridge, and Paintbrush Canyon faults, perhaps triggered by caldera collapse and increased vertical loading associated with the newly deposited tuff sheet, is a strong candidate for perturbing the regional stress field; *(e)* formation of the northeast-striking joints with orientation controlled by the perturbed stress field in response to gas pressure during fumarolic activity; *(f)* formation of the northwest-striking joints controlled by a stress switch due to the presence of the extensive northeast-striking joint swarms in response to gas pressure and possibly aided by differential compaction across the northwest-trending basin; and *(g)* tube formation on both joint sets during degassing and lithophysae formation in the upper Tiva Canyon Tuff. Modeling of fault-controlled stress-field perturbation does not completely exclude other possible contributions to perturbation of the local stress field. For example, with appropriate data, the roles of differential compaction and thermal gradients could be explicitly assessed. Similarly, a better understanding of the role of caldera collapse in perturbing stress fields and triggering fault motions might provide a sufficient basis for a quantitative analysis of this possibility. Nonetheless, we think that this contribution represents a useful first attempt to relate the roles of caldera collapse, ignimbrite deposition and cooling, and fault behavior and joint development to explain the origin of a joint network with a very interesting formation history. This interpretation also illustrates that a series of stress sources acting at a variety of scales, time spans, and magnitudes can combine to produce an apparently simple orthogonal joint geometry.

3. This new interpretation subdivides previously interpreted cooling joints into prelithophysae tube-bearing joints related to gas escape and postlithophysae joints without tubes related to thermoelastic contraction. Conclusive identification of contractional cooling joints depends on relating fracture attributes to processes during ignimbrite lithification.

4. Our conclusions regarding very early development of tube-bearing joints applies to such joints throughout the Paintbrush Group. Tube-bearing joints change the characteristics of the fracture geometry in a volume of lithophysae-bearing rock by adding persistent, planar, closely spaced fractures with preferred orientations to the system. Northwest and northeast strikes of joint sets in both the Tiva Canyon and Topopah Spring Tuffs indicate that stress-field perturbation was a recurrent process during the deposition and cooling of both welded ignimbrite units of the Paintbrush Group.

Downloaded from gsabulletin.gsapubs.org on November 12, 2010


## ACKNOWLEDGMENTS

This paper was prepared to document work performed by the Center for Nuclear Waste Regulatory Analyses (CNWRA) for the U.S. Nuclear Regulatory Commission (NRC) under Contracts Nos. NRC-02-97-009 and NRC-02-02-012. The activities reported here were performed on behalf of the NRC Office of Nuclear Material Safety and Safeguards, Division of Waste Management. The report is an independent product of the CNWRA and does not necessarily reflect the views or regulatory position of the NRC. We thank James P. Hogan for assistance in the field and Rebecca Emmot for assistance with manuscript preparation. Acknowledgment is made to the Rock Fracture Project, Stanford University, for use of Poly3D and Poly3DGUI. Critical reviews by Terry Engelder, James P. Evans, Philip Justus, Wesley C. Patrick, Chris Potter, Larry McKague, and Wanda Taylor greatly improved the manuscript.

## REFERENCES CITED

Abe, K., 1992, Seismicity of the caldera-making eruption of Mount Katmai, Alaska, in 1912: Bulletin of the Seismological Society of America, v. 82, p. 175–191.

Albin, A.L., Singleton, W.L., Moyer, T.C., Lee, A.C., Lung, R.C., Eatman, G.L.W., and Barr, D.L., 1997, Geology of the Main Drift—Station 28 + 00 to 55 + 00, Exploratory Studies Facility, Yucca Mountain Project, Yucca Mountain, Nevada: Summary Report by the U.S. Bureau of Reclamation to the U.S. Department of Energy, DTN GS970208314224. 005.

Axen, G.J., Taylor, W.J., and Bartlet, J.M., 1993, Space-time patterns and tectonic controls of Tertiary extension and magmatism in the Great Basin of the western United States: Geological Society of America Bulletin, v. 105, p. 56–76.

Bai, T., Maerten, L., Gross, M.R., and Aydin, A., 2002, Orthogonal cross joints: Do they imply a regional stress rotation?: Journal of Structural Geology, v. 24, p. 77–88.

Banks, N.G., and Hoblitt, R.P., 1981, Summary of temperature studies of 1980 deposits, *in* Lipman, P.W., and Mullineaux, D.R., ed., The 1980 eruptions of Mount St. Helens, Washington: U.S. Geological Survey Professional Paper 1250, p. 295–314.

Barton, C.C., and Larsen, E., 1985, Fractal geometry of two-dimension fracture networks at Yucca Mountain, *in* Stephanson, O., ed., Proceedings of the International Symposium on Fundamentals of Rock Joints, Sweden: Lulea, Sweden, Centek Publishers, p. 77–84.

Barton, C.C., Howard, T.M., and Larsen, E., 1984, Tubular structures on the faces of cooling joints—A new volcanic feature: Eos (Transactions, American Geophysical Union), v. 65, p. 1148.

Barton, C.C., Larsen, E., Page, W.R., and Howard, T.M., 1993, Characterizing fractured rock for fluid-flow, geomechanical, and paleostress modeling: Methods and preliminary results from Yucca Mountain, Nevada: U.S. Geological Survey Open-File Report 93-269, 31 p.

Bierwirth, P.N., 1982, Experimental welding of volcanic ash [B.S. honors thesis]: Victoria, Australia, Monash University, 150 p.

Braunmiller, J., Nblek, J., Leitner, B., and Qamar, A., 1995, The 1993 Klamath Falls, Oregon, earthquake sequence: Source mechanisms from regional data: Geophysical Research Letters, v. 22, p. 105–108.

Buesch, D.C., and Spengler, R.W., 1998, Character of the middle nonlithophysal zone of the Topopah Spring Tuff at Yucca Mountain: High level radioactive waste management, Proceedings of the 1998 International Conference: La Grange Park, Illinois, American Nuclear Society, p. 16–23.

Buesch, D.C., Spengler, R.W., Moyer, T.C., and Geslin, J.K., 1996, Proposed stratigraphic nomenclature and macroscopic identification of lithostratigraphic units of the Paintbrush Group exposed at Yucca Mountain, Nevada: U.S. Geological Survey Open-File Report 94-469, 45 p.

Buesch, D.C., Beason, S.C., and Spengler, R.W., 1999, Relations among welding, vapor-phase activity, crystallization, and fractures in the Tiva Canyon and Topopah Spring Tuffs, at Yucca Mountain: Geological Society of America Abstracts with Programs, v. 31, no. 7, p. A476–A477.

Bursik, M.I., and Woods, A.W., 1996, The dynamics and thermodynamics of large ash flows: Bulletin of Volcanology, v. 58, p. 175–193.

Byers, F.M., Jr., Carr, W.J., Orkild, P.P., Quinlivan, W.D., and Sargent, K.A., 1976, Volcanic suites and related cauldrons of the Timber Mountain–Oasis Valley caldera complex: U.S. Geological Survey Professional Paper 919, 70 p.

Caputo, R., 1995, Evolution of orthogonal sets of extension joints: Terra Nova, v. 7, p. 479–490.

Carr, W.J., 1992, Structures in continuously cored, deep drill holes at Yucca Mountain, Nevada, with notes on calcite occurrence: Los Alamos, New Mexico, Sandia National Laboratories, SAND91-7037, 39 p.

Cas, R.A.F., and Wright, J.V., 1987, Volcanic successions: Winchester, Massachusetts, Unwin Hyman Inc, p. 256–258.

Christiansen, R.L., Lipman, P.W., Carr, W.J., Byers, F.M., Jr., Orkild, P.P., and Sargent, K.A., 1977, Timber Mountain–Oasis Valley caldera complex of southern Nevada: Geological Society of America Bulletin, v. 88, p. 943–959.

Comninou, M., and Dundurs, J., 1975, The angular dislocation in a half space: Journal of Elasticity, v. 5, p. 205–216.

Crider, J.G., 2001, Oblique slip and the geometry of normal-fault linkage: Mechanics and a case study from the Basin and Range in Oregon: Journal of Structural Geology, v. 23, p. 1997–2009.

Crider, J.G., and Pollard, D.D., 1998, Fault linkage: Three-dimensional mechanical interaction between echelon normal faults: Journal of Geophysical Research, v. 103, p. 24,373–24,391.

Crider, J.G., Schaff, D.P., Pollard, D.D., and Beroza, G.C., 2001, Considering the third dimension in stress-triggering of aftershocks: 1993 Klamath Falls (OR) earthquake sequence: Geophysical Research Letters, v. 28, p. 2739–2742.

Crouch, S.L., and Starfield, A.M., 1990, Boundary element methods in solid mechanics: Boston, Unwin Hyman, 237 p.

CRWMS M and O (Civilian Radioactive Waste Management System Management and Operating Contractor), 1998, Geology of the Exploratory Studies Facility—Topopah Spring Loop: Las Vegas, Nevada, BAB000000-0117-0200-00002 REV 01, 44 p.

CRWMS M and O (Civilian Radioactive Waste Management System Management and Operating Contractor), 2000, Fracture geometry analysis for the stratigraphic units of the repository host horizon: Las Vegas, Nevada, ANL-EBS-GE-000006 REV 00, 62 p.

Day, W.C., Dickerson, R.P., Potter, C.J., Sweetkind, D.S., San Juan, C.A., Drake, R.M., II, and Fridrich, C.J., 1998a, Geologic map of the Yucca Mountain area, Nye County, Nevada: U.S. Geological Survey Miscellaneous Geologic Investigations Series Map I-2627, scale 1:24,000, 1 sheet.

Day, W.C., Potter, C.J., and Sweetkind, D., 1998b, Bedrock geologic map of the central block area, Yucca Mountain, Nye County, Nevada: U.S. Geological Survey Miscellaneous Geologic Investigation Series Map I-2601, scale 1:6000, 2 sheets.

DeGraff, J.M., and Aydin, A., 1987, Surface morphology of columnar joints and its significance to mechanics and direction of joint growth: Geological Society of America Bulletin, v. 99, p. 605–617.

Doser, D.I., 1986, Earthquake processes in the Rainbow Mountain–Fairview Peak–Dixie Valley, Nevada, region 1954–1959: Journal of Geophysical Research, v. 91, p. 12,572–12,586

Dunne, W.M., and North, C.P., 1990, Orthogonal fracture systems at the limits of thrusting: An example from southwestern Wales: Journal of Structural Geology, v. 12, p. 207–215.

Eatman, G.L.W., Singleton, W.L., Moyer, T.C., Barr, D.L., Albin, A.L., Lung, R.C., and Beason, S.C., 1997, Geology of the South Ramp—Station 55 + 00 to 78 + 77, Exploratory Studies Facility, Yucca Mountain Project, Yucca Mountain, Nevada. Milestone SPG42CM3: Denver, Colorado, U.S. Geological Survey, 458 p.

Engelder, T., 1985, Loading path to joint propagation during cycle: An example from the Appalachian Plateau, USA: Journal of Structural Geology, v. 7, p. 459–476.

Engelder, T., and Fischer, M.P., 1996, Loading configurations and driving mechanisms for joints based on the Griffith energy-balance concept: Tectonophysics, v. 256, p. 253–277.

Enlows, H.E., 1955, Welded tuffs of the Chiricahua National Monument, Arizona: Geological Society of America Bulletin, v. 66, p. 1215–1246.

Epstein, B., 1954, Truncated life tests in the exponential case: Annals of Mathematics and Statistics, v. 25, p. 555.

Eyal, Y., and Reches, Z., 1983, Tectonic analysis of the Dead Sea rift region since the Late Cretaceous based on mesostructures: Tectonics, v. 2, p. 167–185.

Fabbri, O., Gaviglio, P., and Gamond, J.-F., 2001, Diachronous development of master joints of different orientations in different lithological units within the same fore-arc basin deposits, Kyushu, Japan: Journal of Structural Geology, v. 23, p. 239–246.

Ferrill, D.A., and Morris, A.P., 2001, Displacement gradient and deformation in normal fault systems: Journal of Structural Geology, v. 23, p. 619–638.

Ferrill, D.A., Stamatakos, J.A., Jones, S.M., Rahe, B., McKague, H.L., Martin, R.H., and Morris, A.P., 1996a, Quaternary slip history of the Bare Mountain fault (Nevada) from the morphology and distribution of alluvial fan deposits: Geology, v. 24, p. 559–562.

Ferrill, D.A., Stirewalt, G.L., Henderson, D.B., Stamatakos, J.A., Morris, A.P., Wernicke, B.P., and Spivey, K.H., 1996b, Faulting in the Yucca Mountain region: Critical review and analyses of tectonic data from the central Basin and Range: U.S. Nuclear Regulatory Commission, CNWRA 95-017, NUREG/CR-6401, 92 p.

Ferrill, D.A., Stamatakos, J.A., and Sims, D., 1999a, Normal fault corrugation: Implications for growth and seismicity of active normal faults: Journal of Structural Geology, v. 21, p. 1027–1038.

Ferrill, D.A., Winterle, J., Wittmeyer, G., Sims, D., Colton, S., Armstrong, A., and Morris, A.P., 1999b, Stressed rock strains groundwater at Yucca Mountain, Nevada: GSA Today, v. 9, no. 5, p. 1–8.

Flint, L.E., and Flint, A.L., 1995, Shallow infiltration processes at Yucca Mountain, Nevada—Neutron logging data 1984–93: U.S. Geological Survey Water-Resources Investigations Report 95-4035, 46 p.

Flint, A.L., Hevesi, J.A., and Flint, L.E., 1996, Conceptual and numerical model of infiltration for the Yucca Mountain area, Nevada, Yucca Mountain Milestone 3GU1623M, Denver, Colorado: U.S. Geological Survey, 174 p.

Fridrich, C.J., 1999, Tectonic evolution of the Crater Flat basin, Yucca Mountain region, Nevada, *in* Wright, L., and Troxel, B., eds., Cenozoic basins of the Death Valley region: Geological Society of America Special Paper 333, p. 169–195.

Friedman, I., Long, W., and Smith, R.L., 1963, Viscosity and water content of rhyolite glass: Journal of Geophysical Research, v. 68, p. 6522–6535.

Frizzell, V.A., and Shulters, J., 1990, Geologic map of the Nevada Test Site, southern Nevada: U.S. Geological Survey Miscellaneous Geologic Investigations Series Map I-2046, 1:100,000 scale.

Gross, M.R., 1993, The origin and spacing of cross joints: Examples from the Monterey Formation, Santa Barbara coastline, California: Journal of Structural Geology 15, p. 737–751.

Gross, M.R., Fischer, M.P., Engelder, T., and Greenfield, R.J., 1995, Factors controlling joint spacing in interbedded sedimentary rocks: Integrating numerical models with field observations from the Monterey Formation, U.S.A., *in* Ameen, M.S., ed., Fractography: Fracture topography as a tool in fracture mechanics and stress analysis: Geological Society [London] Special Publication 92, p. 215–233.

Hancock, P.L., 1985, Brittle microtectonics: Principles and

Downloaded from gsabulletin.gsapubs.org on November 12, 2010


practice: Journal of Structural Geology, v. 7, p. 437–457.

Hauksson, E., Hutton, K., Kanamori, H., Jones, L., Mori, J., Hough, S., and Roquemore, G., 1995, Preliminary report on the 1995 Ridgecrest earthquake sequence in eastern California: Seismological Research Letters, v. 66, p. 54–60.

Hildreth, W., 1983, The compositionally zoned eruption of 1912 in the Valley of Ten Thousand Smokes, Katmai National Park, Alaska: Journal of Volcanology and Geothermal Research, v. 18, p. 1–56.

Hobbs, D.W., 1967, The formation of tension joints in sedimentary rocks: An explanation: Geological Magazine, v. 104, p. 550–556.

Jeyakumaran, M., Rudnicki, J.W., and Keer, L.M., 1992, Modeling of slip zones with triangular dislocation elements: Bulletin of the Seismological Society of America, v. 82, p. 2153–2169.

Kattenhorn, S.A., Aydin, A., and Pollard, D.D., 2000, Joints at high angles to normal fault strike: An explanation using 3-D numerical models in fault-perturbed stress fields: Journal of Structural Geology, v. 22, p. 1–24.

Keith, T.E.C., 1991, Fossil and active fumaroles in the 1912 eruptive deposits, Valley of Ten Thousand Smokes, Alaska: Journal of Volcanology and Geothermal Research, v. 45, p. 227–254.

Kirsch, G., 1898, Die theorie der elastizitat und die bedurfnisse der festigheitslehre: Zeitschrift des Vereines Deutscher Ingenieure, v. 42, p. 797.

La Pointe, P.R., and Hudson, J.A., 1985, Characterization and interpretation of rock mass joint patterns: Geological Society of America Special Paper 199, 37 p.

Lachenbruch, A.H., 1962, Mechanics of thermal contraction cracks and ice-wedge polygons in permafrost: Geological Society of America Special Paper 70, 65 p.

Lipman, P.W., and Friedman, I., 1975, Interaction of meteoric water with magma: An oxygen-isotope study of ash-flow sheets from southern Nevada: Geological Society of America Bulletin, v. 86, p. 695–702.

Lofgren, G., 1971, Experimentally produced devitrification textures in natural rhyolitic glass: Geological Society of America Bulletin, v. 82, p. 111–124.

Maerten, L., Gillespie, P., and Pollard, D.D., 2002, Effect of local stress perturbation on secondary fault development: Journal of Structural Geology, v. 24, p. 145–153.

Martel, S., 1994, On the paradox of systematic, contemporaneous, orthogonal opening-mode fractures, *in* Nelson, R., and Laubach, S., eds., Rock mechanics: Rotterdam, Netherlands, Balkema, p. 801–808.

Mauldon, M., Dunne, W.M., and Rohrbaugh, M.R., 2001, Circular scanlines and circular windows: New tools for characterizing the geometry of fracture traces: Journal of Structural Geology, v. 23, p. 247–258.

Miller, T.F., 1990, A numerical model of volatile behavior in nonwelded cooling pyroclastic deposits: Journal of Geophysical Research, v. 95, p. 19,349–19,364.

Mongano, G.S., Singleton, W.L., Moyer, T.C., Beason, S.C., Eatman, G.W., Albin, A.L., and Lung, R.C., 1999, Geology of the ECRB Cross Drift—Exploratory Studies Facility, Yucca Mountain Project, Yucca Mountain, Nevada. Milestone SPG42GM3: Denver, Colorado, U.S. Geological Survey, 46 p.

Monsen, S.A., Carr, M.D., Reheis, M.C., and Orkild, P.P., 1992, Geologic map of Bare Mountain, Nye County, Nevada: U.S. Geological Survey Miscellaneous Geologic Investigations Series Map 2201, 1:24,000 scale.

Morgan, T.L., 1984, Fracture characterization in the Tiva Canyon Member, Paintbrush Tuff, Yucca Mountain [M.S. thesis]: Fort Collins, Colorado, Colorado State University, 120 p.

Morris, A.P., Ferrill, D.A., and Henderson, D.B., 1996, Slip tendency analysis and fault reactivation: Geology, v. 24, p. 275–278.

Nostro, C., Stein, R.S., Cocco, M., Belardinelli, M.E., and Marzocchi, W., 1998, Two-way coupling between Vesuvius eruptions and southern Apennine earthquakes (Italy) by elastic stress transfer: Journal of Geophysical Research, v. 103, p. 24,487–24,504.

Odling, N.E., Gillespie, P., Bourgine, B., Castaing, C., Chiles, J.-P., Christensen, N.P., Fillion, E., Genter, A., Olsen, C., Thrane, L., Trice, R., Aarseth, E., Walsh, J.J., and Watterson, J., 1999, Variations in fracture system geometry and their implications for fluid flow in fractured hydrocarbon reservoirs: Petroleum Geoscience, v. 5, p. 373–384.

Olson, J.E., 1996, Post-compressional relaxation and orthogonal fracture pattern development: Geological Society of America Abstracts with Programs, v. 28, no. 1, p. 56.

Pollard, D.D., and Aydin, A., 1988, Progress in understanding jointing over the past century: Geological Society of America Bulletin, v. 100, p. 1181–1204.

Potter, C.J., Dickerson, R.P., Sweetkind, D.S., Drake, R.M., II, Taylor, E.M., Fridrich, C.J., San Juan, C.A., and Day, W.C., 2002, Geologic map of the Yucca Mountain region, Nye County, Nevada: U.S. Geological Survey Miscellaneous Geologic Investigations Series Map I-2755, scale 1:50,000, 37 p. pamphlet.

Priest, S.D., 1993, Discontinuity analysis for rock engineering: New York, Chapman and Hall, 527 p.

Ragan, D.M., and Sheridan, M.F., 1972, Compaction of the Bishop Tuff, California: Geological Society of America Bulletin, v. 83, p. 95–106.

Rawnsley, K.D., Rives, T., Petit, J.-P., Hencher, S.R., and Lumsden, A.C., 1992, Joint development in perturbed stress fields near faults: Journal of Structural Geology, v. 20, p. 1641–1661.

Rawnsley, K.D., Peacock, D.C.P., Rives, T., and Petit, J.-P., 1998, Joints in the Mesozoic sediments around the Bristol Channel Basin: Journal of Structural Geology, v. 20, p. 1641–1661.

Riehle, J.R., 1973, Calculated compaction profiles of rhyolitic ash-flow tuffs: Geological Society of America Bulletin, v. 84, p. 2193–2216.

Riehle, J.R., Miller, T.F., and Baley, R.A., 1995, Cooling, degassing and compaction of rhyolitic ash flow tuffs: A computational model: Bulletin of Volcanology, v. 57, p. 319–336.

Rives, T., Rawnsley, K.D., and Petit, J.-P., 1994, Analogue simulation of natural orthogonal joint set formation in brittle varnish: Journal of Structural Geology, v. 16, p. 419–429.

Rosenbaum, J.G., 1986, Paleomagnetic directional dispersion produced by plastic deformation in a thick Miocene welded tuff, southern Nevada: Implications for welding temperatures: Journal of Geophysical Research, v. 91, p. 12,817–12,834.

Rosenbaum, J.G., 1993, Magnetic grain-size variations through an ash flow sheet: Influence on magnetic properties and implications for cooling history: Journal of Geophysical Research, v. 98, p. 11,715–11,727.

Ross, C.S., and Smith, R.L., 1961, Ash-flow tuffs: Their origin, geologic relations and identification: U.S. Geological Survey Professional Paper 366, 81 p.

Sawyer, D.R., Fleck, R.J., Lanphere, M.A., Warren, R.G., Broxton, D.E., and Hudson, M.R., 1994, Episodic caldera volcanism in the Miocene southwestern Nevada volcanic field: Revised stratigraphic framework, $^{40}Ar/^{39}Ar$ geochronology, and implications for magmatism and extension: Geological Society of America Bulletin, v. 106, p. 1304–1318.

Scott, R.B., 1990, Tectonic setting of Yucca Mountain, southwest Nevada: Geological Society of America Memoir 176, p. 251–282.

Scott, R.B., and Bonk, J., 1984, Preliminary geologic map of Yucca Mountain, Nye County, Nevada, with geologic sections: U.S. Geological Survey Open-File Report 84-494, 1:12,000.

Secor, D.T., 1968, Mechanics of natural extension fracturing at depth in the Earth's crust, *in* Baer, A.J., and Norris, D.K., eds., Proceedings, Conference on Research in Tectonics, Ottawa 1968: Geological Survey of Canada Paper 68-52, p. 3–48.

Sheridan, M.F., 1970, Fumarolic mounds and ridges of the Bishop Tuff, California: Geological Society of America Bulletin, v. 81, p. 851–868.

Smith, R.L., 1960, Zones and zonal variations in welded ash flows: U.S. Geological Survey Professional Paper 354-F, 11 p.

Stauffer, M.R., and Gendzwill, D.J., 1987, Fractures in the northern plains, stream patterns and mid-continent stress field: Canadian Journal of Earth Sciences, v. 24, p. 1086–1097.

Stock, J.M., Healy, J.H., Hickman, S.H., and Zoback, M.D., 1985, Hydraulic fracturing stress management at Yucca Mountain, Nevada, and relationship to the regional stress field: Journal of Geophysical Research, v. 90, p. 8691–8706.

Sweetkind, D.S., and Williams-Stroud, S.C., 1996, Characteristics of fractures at Yucca Mountain, Nevada: Synthesis report: U.S. Geological Survey Administrative Report, 91 p.

Sweetkind, D.S., Verbeek, E.R., Geslin, J.K., and Moyer, T.C., 1995a, Fracture character of the Paintbrush Tuff nonwelded hydrologic unit, Yucca Mountain, Nevada: U.S. Geological Survey Administrative Report, 202 p.

Sweetkind, D.S., Verbeek, E.R., Singer, F.R., Byers, F.M., and Martin, L.G., 1995b, Surface fracture network at pavement P2001, Fran Ridge, near Yucca Mountain, Nye County, Nevada: U.S. Geological Survey Administrative Report, 130 p.

Sweetkind, D.S., Beason, S.C., and Buesch, D.C., 2003, Overview of the stratigraphic and structural setting of Yucca Mountain, Nevada, U.S.A.: International Journal of Rock Mechanics (in press).

Thomas, A.L., 1993, Poly3D: A three-dimensional, polygonal element, displacement discontinuity boundary element computer program with applications to fractures, faults and cavities in the Earth's crust [M.S. thesis]: Stanford, California, Stanford University, 97 p.

Throckmorton, C.K., and Verbeek, E.R., 1995, Joint networks in the Tiva Canyon and Topopah Spring Tuffs of the Paintbrush Group, southwestern Nevada: U.S. Geological Survey, Open-File Report 95-2, 179 p.

Ver Steeg, K., 1942, Jointing in coal beds of Ohio: Economic Geology, v. 37, p. 503–509.

Wernicke, B., 1992, Cenozoic extensional tectonics of the U.S. Cordillera, *in* Burchfiel, B.C., Lipman, P.W., and Zoback, M.L., eds., The Cordilleran orogen: Conterminous United States: Boulder, Colorado, Geological Society of America, Geology of North America, v. G-3, p. 553–581.

Willemse, E.M.J., Pollard, D.D., and Aydin, A., 1996, Three-dimensional analysis of slip distributions on normal fault arrays, with consequences for fault scaling: Journal of Structural Geology, v. 18, p. 295–309.

Winograd, I.J., 1971, Hydrogeology of ash flow tuff: A preliminary statement: Water Resources Research, v. 7, p. 994–1006.

Young, S.R., Stirewalt, G., and Morris, A.P., 1992, Geometric models of faulting at Yucca Mountain, *in* Hossain, Q.A., ed., Dynamic analysis and design considerations for high level nuclear waste repositories: New York, American Society of Civil Engineers, p. 97–117.

Zoback, M.L., Anderson, R.E., and Thompson, G.A., 1981, Cainozoic evolution of the state of stress and style of tectonism of the Basin and Range province of the western United States: Royal Society of London Philosophical Transactions, Ser. A, v. 300, p. 407–434.

Manuscript Received by the Society 7 August 2002
Revised Manuscript Received 18 April 2003
Manuscript Accepted 19 May 2003

Printed in the USA